Holographic charged fluid with chiral electric separation effect

Yanyan Bu,[a] **Rong-Gen Cai,**[b,c] **Qing Yang**[d] **and Yun-Long Zhang**[e,f]

[a]*Department of Physics, Harbin Institute of Technology,*
92 West Dazhi Street, Nan Gang District, Harbin 150001, China

[b]*CAS Key Laboratory of Theoretical Physics, Institute of Theoretical Physics,*
Chinese Academy of Sciences,
Zhong Guan Cun East Street 55, P.O. Box 2735, Beijing 100190, China

[c]*School of Physical Sciences, University of Chinese Academy of Sciences,*
19(A) Yuquan Road, Shijingshan District, Beijing 100049, China

[d]*Department of Astronomy, Beijing Normal University,*
19 Xin Jie Kou Wai Street, Haidian District, Beijing 100875, China

[e]*Asia Pacific Center for Theoretical Physics, APCTP Headquarters,*
67 Cheongam-ro, Hyoja-dong, Nam-gu, Pohang 790-784, Korea

[f]*Center for Quantum Spacetime (CQUeST), Sogang University,*
35 Baekbeom-ro, Sinsu-dong, Mapo-gu, Seoul 121-742, Korea

E-mail: yybu@hit.edu.cn, cairg@itp.ac.cn, yangqing@bnu.edu.cn, yunlong.zhang@apctp.org

ABSTRACT: Hydrodynamics with both vector and axial currents is under study within a holographic model, consisting of canonical $U(1)_V \times U(1)_A$ gauge fields in an asymptotically AdS$_5$ black brane. When gravitational back-reaction is taken into account, the chiral electric separation effect (CESE), namely the generation of an axial current as the response to an external electric field, is realized naturally. Via fluid/gravity correspondence, all the first order transport coefficients in the hydrodynamic constitutive relations are evaluated analytically: they are functions of vector chemical potential μ, axial chemical potential μ_5 and the fluid's temperature T. Apart from the proportionality factor $\mu\mu_5$, the CESE conductivity is found to be dependent on the dimensionless quantities μ/T and μ_5/T nontrivially. As a complementary study, frequency-dependent transport phenomena are revealed through linear response analysis, demonstrating perfect agreement with the results obtained from fluid/gravity correspondence.

Contents

1 Introduction

Fluid dynamics is an effective low energy description of most interacting systems at finite temperature. Within such a hydrodynamic approximation, the entire dynamics of a microscopic theory is reduced to that of macroscopically conserved currents, such as the stress-energy tensor and charge current operators computed in a locally near equilibrium thermal state. An essential ingredient of any fluid dynamics is the constitutive relations which relate the macroscopically conserved currents to the hydrodynamic variables, such as fluid velocity and charge densities, and to external forces like external electromagnetic fields. Derivative expansion in the hydrodynamic variables and external forces accounts for deviations from thermal equilibrium. At each order, the derivative expansion is fixed by thermodynamics and symmetries, up to a finite number of transport coefficients such as viscosity and diffusion coefficients. These transport coefficients are not calculable from hydrodynamics itself but have to be deduced experimentally or computed from the underlying microscopic theory.

For relativistic fluid dynamics, the stress-energy tensor is conveniently parameterized as

$$T_{\mu\nu} = \mathcal{E} u_\mu u_\nu + \mathcal{P} P_{\mu\nu} + \pi_{\mu\nu}, \tag{1.1}$$

where $u_\mu, \mathcal{E}, \mathcal{P}$ are the velocity, energy density and pressure of the fluid, and $P_{\mu\nu} = u_\mu u_\nu + \eta_{\mu\nu}$ is the projection tensor. Up to the first order in the derivative expansion, the viscous component $\pi_{\mu\nu}$ takes the form,

$$\pi_{\mu\nu} = -\eta P_\mu^\alpha P_\nu^\beta \left(\partial_\alpha u_\beta + \partial_\beta u_\alpha - \frac{2}{3} P_{\alpha\beta} \partial_\sigma u^\sigma \right) - \zeta P_{\mu\nu} \partial_\alpha u^\alpha + \mathcal{O}(\partial^2), \qquad (1.2)$$

where η, ζ are the shear viscosity and bulk viscosity, respectively. Throughout this work we will take the Landau-Lifshitz frame so that $u^\mu \pi_{\mu\nu} = 0$.

For the fluid with conserved charges, one also needs to specify constitutive relations for the associated currents. Indeed, the charge transport properties are found to be useful in probing the structure and dynamics of matter. A well-known example is the Ohm's law $J^i \equiv \langle \bar{\psi} \gamma^i \psi \rangle = \sigma E^i$, which states the generation of an electric current in response to an external electric field for a normal conducting media. In recent years, exploration of other possible electric current generation, particularly for a system with charged chiral fermions, has attracted much interest. It turns out that the celebrated microscopic chiral anomaly induces fascinating anomalous transport phenomena that break the space parity symmetry. One such example is the chiral magnetic effect (CME) [1–4]: generation of an electric current directed along an externally applied magnetic field, $\vec{J} = \xi_B \vec{B}$. The existence of CME relies on chirality imbalance between left- and right-handed chiral fermions, usually parameterized by an axial chemical potential μ_5. For a rotating hydrodynamic flow, chiral anomaly induces a vector current along the fluid vorticity, $\vec{J} = \frac{1}{2} \xi \vec{\nabla} \times \vec{u}$, which is called the chiral vortical effect (CVE) [5–7].

On the other hand, an axial current $J_5^i \equiv \langle \bar{\psi} \gamma^i \gamma_5 \psi \rangle$ also exists for a system with charged chiral fermions. In fact, via the chiral anomaly effect, an axial current is generated along an external magnetic field, $\vec{J}_5 = \xi_{5B} \vec{B}$, which is referred to as chiral separation effect (CSE) [8, 9]. Interestingly, the interplay of CME and CSE predicts a gapless wave mode propagating along the magnetic field, called chiral magnetic wave (CMW) [10]. In heavy-ion collisions, the CMW induces an electric quadrupole moment of the quark-gluon plasma [11], leaving experimentally observable effects [11–14]. It is important to stress that chiral anomaly-induced transport phenomena summarized above are non-dissipative [7], that is they do not contribute to entropy production. While observable signatures predicted by the CME have not been conclusively detected in heavy-ion collisions [15–18], the CME may explain a large negative magneto-resistance observed in Dirac and Weyl semi-metals [19–21]. We recommend recent reviews [22–27] and references therein on the subject of anomalous transport phenomena.

The separation of chiral charge could also be induced by an external electric field, $\vec{J}_5 = \sigma_{5e} \vec{E}$, which is called chiral electric separation effect (CESE) [28, 29]. However, it is important to emphasize that the CESE does not originate from chiral anomaly but is simply the result of conduction of a chiral many-body environment [28]. On very general grounds, the CESE exists only when both vector and axial chemical potentials are nonzero. Based on Kubo formula, the CESE conductivity has been computed for thermal quantum electrodynamics (QED) [28] and quantum chromodynamics (QCD) plasmas [29] at high-temperature regime up to leading-log order in gauge couplings. In the strongly-coupled

regime, the CESE was studied in [30, 31] by using the holographic QCD model of [32, 33]. Recently, the CESE conductivity is also computed within the framework of kinetic theory [34–37] under the relaxation time approximation (RTA). If the CESE conductivity is parameterized as $\sigma_{5e} = \mu\mu_5\tilde{\chi}_A$, then all these studies indicate that $\tilde{\chi}_A$ depends on μ, μ_5 weakly. In analogy with CMW, the CESE, combined with the Ohm's law, results in a new gapless wave mode propagating along the electric field, which is called density wave [28] or chiral electric wave (CEW) [31].

The transport phenomena reviewed above could be summarized into hydrodynamic constitutive relations for vector and axial currents. In the Landau-Lifshitz frame where $u_\mu J^\mu = -\rho$ and $u_\mu J_5^\mu = -\rho_5$, we are ended up with [38–40],

$$J^\mu = \rho u^\mu + \sigma_e\left[E^\mu - TP^{\mu\nu}\partial_\nu\left(\frac{\mu}{T}\right)\right] - \tilde{\sigma}_{5e}TP^{\mu\nu}\partial_\nu\left(\frac{\mu_5}{T}\right) + (\xi\omega^\mu + \xi_B B^\mu) + \mathcal{O}(\partial^2), \qquad (1.3)$$

$$J_5^\mu = \rho_5 u^\mu + \sigma_{5e}\left[E^\mu - TP^{\mu\nu}\partial_\nu\left(\frac{\mu}{T}\right)\right] - \tilde{\sigma}_e TP^{\mu\nu}\partial_\nu\left(\frac{\mu_5}{T}\right) + (\xi_5\omega^\mu + \xi_{5B} B^\mu) + \mathcal{O}(\partial^2), \qquad (1.4)$$

where ρ, ρ_5 are vector and axial charge densities. The external electromagnetic fields E^μ, B^μ and the fluid's vorticity ω^μ are

$$E^\mu \equiv F_{(\epsilon)}^{\mu\nu}u_\nu, \qquad B^\mu \equiv \frac{1}{2}\epsilon^{\mu\nu\alpha\beta}u_\nu F_{\alpha\beta}^{(\epsilon)}, \qquad \omega^\mu \equiv \frac{1}{2}\epsilon^{\mu\nu\alpha\beta}u_\nu\partial_\alpha u_\beta. \qquad (1.5)$$

In (1.3)(1.4), the Wiedemann-Franz law has been used to relate thermal conductivity to electrical conductivity. The $\tilde{\sigma}_{5e}$- and $\tilde{\sigma}_e$-terms are relevant to chiral charge diffusions, while ξ_5-term is an axial analogue of CVE. Time/space evolution of the system is determined by solving the hydrodynamic equations

$$\partial^\mu T_{\mu\nu} = J^\alpha F_{\nu\alpha}^{(\epsilon)}, \qquad \partial_\mu J^\mu = 0, \qquad \partial_\mu J_5^\mu = \mathcal{C}E_\mu B^\mu, \qquad (1.6)$$

where the axial current is not conserved due to chiral anomaly effect and $\mathcal{C}$ denotes the anomaly coefficient. $\xi, \xi_5, \xi_B, \xi_{5B}$-terms are chiral anomaly-induced and correspond to non-dissipative transport phenomena, particularly making zero entropy production. In contrast, $\sigma_e, \sigma_{5e}, \tilde{\sigma}_e, \tilde{\sigma}_{5e}$ are dissipative transport coefficients and have to be determined by the underlying microscopic theory and will be the focus of present work.

We would like to point out that studies in references [28–31] were carried out under the *decoupling limit* (or *probe limit*), where the vector and axial currents were taken as decoupled from the stress-energy tensor of the fluid. While the decoupling limit allows deriving a simple Kubo formula for CESE conductivity, it does result in loss of some important physical contents, such as a pole in DC electrical conductivity due to spatial translation invariance [41–43]. In the probe limit, the authors of [30, 31] found a nonzero CESE conductivity for the holographic QCD model, which consists of probe $D8/\overline{D}8$-branes in the background geometry of N_c stacks of $D4$-brane. A crucial point of [30, 31] in realizing CESE is about the *explicit interaction* between the vector and axial gauge fields in the bulk, which originates from the nonlinear Dirac-Born-Infeld (DBI) action on the world-volumes of $D8/\overline{D}8$. Indeed, it was found that the CESE conductivity does vanish in a simple holographic setup with canonical $\mathrm{U}(1)_V \times \mathrm{U}(1)_A$ Maxwell fields *probing* the fixed Schwarzschild-AdS$_5$ background [44–46].

In this work, we reconsider the holographic $U(1)_V \times U(1)_A$ model and take into account the gravitational back-reaction effect on the gauge sectors of the bulk theory. While the anomaly coefficient $\mathcal{C}$ is fixed by the microscopic theory, we will take it as a free parameter and turn it off for the present study. Equivalently, the bulk Chern-Simons actions will be neglected in the holographic setup of [44–46]. Note that there is no explicit interaction between $U(1)_V$ and $U(1)_A$ gauge fields in the bulk action. However, as will be clear later, the gravitational back-reaction will result in a coupling between perturbations of $U(1)_V$ and $U(1)_A$ bulk fields. This is the mechanism of generating CESE in such a simple holographic model. In the next subsection, we will summarize the results and make the comparison with previous works. The remaining sections supplement all calculational details.

1.1 Summary of the results

Except for those chiral anomaly-induced terms, we will re-derive the first order constitutive relations (1.1), (1.3), (1.4) via fluid/gravity correspondence [47]. For a specific holographic model to be introduced in section 2, we analytically compute all dissipative transport coefficients. The calculational details will be presented in section 3. The shear and bulk viscosities in (1.2) take universal values of holographic conformal fluids (holographically described by two-derivative Einstein gravity),

$$\eta = \frac{1}{4\pi}s, \qquad \zeta = 0, \qquad (1.7)$$

where s is the entropy density of the dual fluid.

The dissipative transport coefficients in (1.3) and (1.4) could be presented in several different forms. In the first form, they are

$$\sigma_e = \frac{\sigma_Q \mu^2 + \sigma_0 \mu_5^2}{\mu^2 + \mu_5^2}, \qquad \sigma_{5e} = \tilde{\sigma}_{5e} = \mu\mu_5 \frac{\sigma_Q - \sigma_0}{\mu^2 + \mu_5^2}, \qquad \tilde{\sigma}_e = \frac{\sigma_Q \mu_5^2 + \sigma_0 \mu^2}{\mu^2 + \mu_5^2}, \qquad (1.8)$$

where σ_Q and σ_0 are given by

$$\sigma_Q \equiv \frac{\sigma_0 (Ts)^2}{(Ts + \mu\rho + \mu_5\rho_5)^2} = \frac{\sigma_0 (Ts)^2}{(\mathcal{E} + \mathcal{P})^2}, \qquad \sigma_0 \equiv \frac{\pi T}{2}\left(1 + \sqrt{1 + \frac{2}{3}\frac{\mu^2 + \mu_5^2}{\pi^2 T^2}}\right). \qquad (1.9)$$

It is important to stress that σ_e, σ_{5e} and $\tilde{\sigma}_e, \tilde{\sigma}_{5e}$ are *intrinsic* conductivities, which are usually referred to as "quantum critical" [48] or "incoherent" [49, 50] conductivities in holographic framework. We have reserved the notation σ_Q to the intrinsic electrical conductivity for the single charge case, since $\sigma_e = \sigma_Q$ once $\rho_5 = 0$ or $\mu_5 = 0$. In the probe limit where $\mu = \mu_5 = 0$, we have $\sigma_e = \tilde{\sigma}_e = \sigma_0 = \pi T$, but $\sigma_{5e}, \tilde{\sigma}_{5e}$ vanish.

In (1.8), the relation $\sigma_{5e} = \tilde{\sigma}_{5e}$ originates from Onsager reciprocal relation for a time-reversal symmetric system. Additionally, there are mirror symmetric relations $\sigma_e \leftrightarrow \tilde{\sigma}_e$ and $\sigma_{5e} \leftrightarrow \tilde{\sigma}_{5e}$ under the exchange $\mu \leftrightarrow \mu_5$, which are specific to our holographic model.[1] Thanks to these symmetric relations, in the discussions below we will focus on σ_e, σ_{5e}. As will be clear in section 4, these symmetric relations for DC transport coefficients are extendable to associated alternating current (AC) conductivities in (4.13). While the second law

---

[1]We thank Yan Liu for stimulating discussions on this issue.

of thermodynamics, i.e., non-negativeness of divergence for the entropy current, could not fix the values of dissipative transport coefficients, it does set constraints for them [29, 30],

$$\sigma_e \geq 0, \qquad \tilde{\sigma}_e \geq 0, \qquad \sigma_e \tilde{\sigma}_e \geq \sigma_{5e} \tilde{\sigma}_{5e}, \qquad (1.10)$$

which are obviously satisfied by our results (1.8)(1.9).

From the dual fluid's point of view, it is more natural to re-express $\sigma_e, \tilde{\sigma}_e, \sigma_{5e}, \tilde{\sigma}_{5e}$ in terms of chemical potentials and temperature. As a result, (1.8) are turned into

$$\sigma_e = \pi T \frac{2\gamma + (3\gamma - 1)\bar{\mu}_5^2}{2(3\gamma - 2)^2} \equiv T\chi_V, \qquad \sigma_{5e} = -\pi T \bar{\mu}\bar{\mu}_5 \frac{3\gamma - 1}{2(3\gamma - 2)^2} \equiv T\bar{\mu}\bar{\mu}_5\chi_A, \qquad (1.11)$$

where

$$\gamma(\bar{\mu}, \bar{\mu}_5) = \frac{1}{2}\left(1 + \sqrt{1 + \frac{2}{3}(\bar{\mu}^2 + \bar{\mu}_5^2)}\right), \qquad \bar{\mu} = \frac{\mu}{\pi T}, \qquad \bar{\mu}_5 = \frac{\mu_5}{\pi T}. \qquad (1.12)$$

In (1.11) we defined χ_A to measure deviation of the CESE conductivity σ_{5e} from the conjectured universal factor $T\bar{\mu}\bar{\mu}_5$ [28, 29]. We also defined χ_V to measure deviation of the Ohmic conductivity σ_e from its probe limit. In the high temperature (small chemical potential) limit or low temperature (large chemical potential) limit, the conductivities (1.11) behave as,

$$
\begin{aligned}
\sigma_e &\simeq \pi T, & \sigma_{5e} &\simeq -\pi T\bar{\mu}\bar{\mu}_5, & \bar{\mu}, \bar{\mu}_5 &\ll 1, \\
\sigma_e &\simeq \frac{\pi T \bar{\mu}_5^2}{\sqrt{6(\bar{\mu}^2 + \bar{\mu}_5^2)}}, & \sigma_{5e} &\simeq -\frac{\pi T\bar{\mu}\bar{\mu}_5}{\sqrt{6(\bar{\mu}^2 + \bar{\mu}_5^2)}}, & \bar{\mu}, \bar{\mu}_5 &\gg 1.
\end{aligned}
\qquad (1.13)
$$

Obviously, only in the high temperature regime where $\bar{\mu}, \bar{\mu}_5 \ll 1$ the CESE conductivity σ_{5e} shows universal behavior as conjectured in [28, 29].

For illustration, in figure 1 we plot $\sigma_e/(\pi T)$ and $-\sigma_{5e}/(\pi T)$ as functions of dimensionless chemical potentials $\bar{\mu}$ and $\bar{\mu}_5$. As seen from figure 1, the axial chemical potential $\bar{\mu}_5$ has the effect of enhancing σ_e while the vector chemical potential $\bar{\mu}$ diminishes it. On the other hand, the CESE conductivity σ_{5e} depends on both $\bar{\mu}$ and $\bar{\mu}_5$ non-trivially. Particularly, the deviation factor χ_A is a monotonic decaying function of $\bar{\mu}$ and $\bar{\mu}_5$. In the high-temperature regime where $\bar{\mu}, \bar{\mu}_5 \ll 1$, the factor χ_A could be thought of as unity, which is obviously violated in the lower temperature limit. In figure 2 we show density plots for the deviation factors χ_V and χ_A.

Below we compare our results with those obtained within various other models [28–31], see table 1. The first two calculations in table 1 were based on perturbative thermal QED and QCD, respectively. To leading-log order in gauge couplings, the conductivities were computed using the Kubo formula in [28, 29]. The rest calculations in table 1 are based on specific holographic models: Sakai-Sugimoto (S-S) model in [30] versus holographic $U(1)_V \times U(1)_A$ model of present work. As shown in table 1, the results obtained from S-S model show the behavior of the pre-factors in $\sigma_e, \sigma_{5e} \propto N_c^2 g_{\rm YM}^2$ [30], which is quite different from those in weakly coupled regime [28, 29]. While in our case, the conductivities depend on the bulk gauge couplings q_V, q_A. If we employ the top-down setups in [52, 53], they
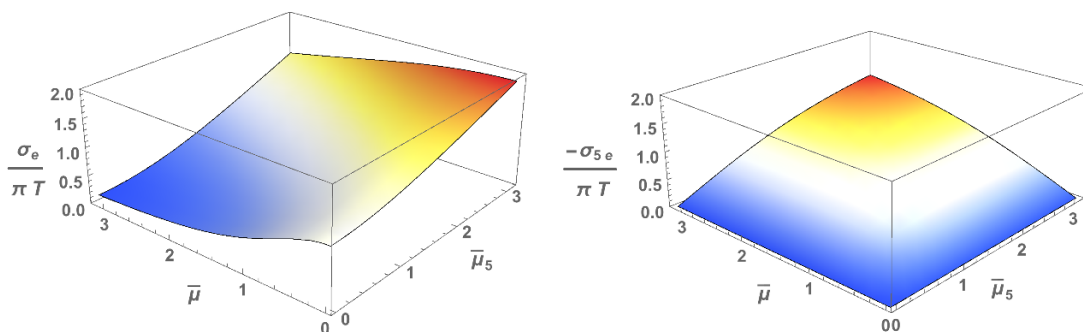
Figure 1. The conductivities $\sigma_e/(\pi T)$ and $-\sigma_{5e}/(\pi T)$ as functions of $\bar{\mu}$ and $\bar{\mu}_5$.
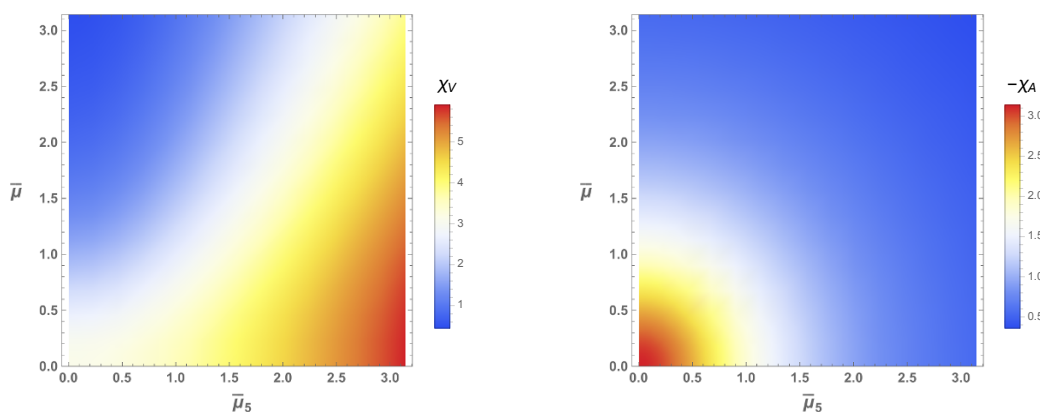

Figure 2. Density plots for χ_V and χ_A in (1.11) as functions of $\bar{\mu}$ and $\bar{\mu}_5$.

could be related to the parameters of boundary theory by $1/q_V^2 \sim 1/q_A^2 \propto N_c N_f/(4\pi^2)$, where N_c and N_f are the numbers of the colors and flavors of the dual theory.

Although these dissipative transport coefficients are model dependent, in the high temperature regime, they do share some universal features, such as the linear dependence in T (for σ_e) and $T\bar{\mu}\bar{\mu}_5$ (for σ_{5e}). In addition, the Ohmic conductivity σ_e has to be positive [28], but the sign of CESE conductivity σ_{5e} could not be fixed by the second law of thermodynamics [28]. Particularly, σ_{5e} was found to be positive for the models in [28–30], but it is shown to be negative from present study (1.11). As shown in table 1, from weak to strong coupling, the conductivities σ_e, σ_{5e} show different dependence on the gauge coupling of boundary gauge theory in various models.

From table 1, in the high temperature regime that $T \gg \mu, \mu_5$, the conductivities in holographic $U(1)_A \times U(1)_V$ model share the same temperature scalings as those in the QED plasma or QGP. The Ohmic conductivity depends linearly on the temperature, $\sigma_e \propto T$, while the CESE conductivity depends inversely on the temperature, $\sigma_{5e} \propto \frac{\mu\mu_5}{T}$. It will become more evident from dimensional analysis as implemented in [29] within relativistic kinetic theory. In the high temperature regime, the conductivities can be expanded in terms of the ratios $\left(\frac{\mu}{T}\right)$ and $\left(\frac{\mu_5}{T}\right)$. To quadratic order in the ratios, the conductivities are constrained to be $\sigma_e \simeq f(T)\left[1 + d_{20}\left(\frac{\mu}{T}\right)^2 + d_{02}\left(\frac{\mu_5}{T}\right)^2\right]$ and $\sigma_{5e} \simeq f(T)d_{11}\left(\frac{\mu}{T}\right)\left(\frac{\mu_5}{T}\right)$,

Pre-factors	QED Plasma [28]	QGP (u,d) [29]	S-S Model [30]	$\mathrm{U}(1)_V \times \mathrm{U}(1)_A$
$\chi_V \equiv \sigma_e/T$	$\frac{15.7}{e^3 \ln(1/e)}$	$13.0 \frac{\mathrm{Tr}_f Q_e Q_V}{g_c^4 \ln(1/g_c)}$	$0.025 \frac{8N_c^2 g_{\mathrm{YM}}^2}{81}$	π/q_V^2 [(1.13)]
$\chi_A \equiv \sigma_{5e}/(T\bar{\mu}\bar{\mu}_5)$	$\frac{20.5}{e^3 \ln(1/e)}$	$14.5 \frac{\mathrm{Tr}_f Q_e Q_A}{g_c^4 \ln(1/g_c)}$	$0.002 \frac{8N_c^2 g_{\mathrm{YM}}^2}{81}$	$-\pi/q_A^2$ [(1.13)]

Table 1. Ohmic and CESE Conductivities in the high temperature regime in various models. *Note.* In this table, e, g_c, g_{YM} are the gauge couplings of QED, QCD, the dual $\mathrm{SU}(N_c)$ gauge theory, respectively. For the calculations in QGP with two light quarks (u,d), $Q_e = \mathrm{Diag}(2/3, -1/3)$, Q_V and Q_A are the vector and axial charge matrices in flavor space. For the S-S model, the results above are read off from relevant numerical plots around $T \simeq 0.2\mathrm{GeV}$ [30]. Indeed, in the high-temperature regime where the chemical potentials are suppressed, $\sigma_e \propto T^2/m_{KK}$ [31, 51], where m_{KK} is the Kaluza-Klein mass in the S-S model. For the results of present study, we have restored the bulk gauge couplings q_V, q_A, which are related to parameters of boundary theory by $1/q_V^2 \sim 1/q_A^2 \propto N_c N_f/(4\pi^2)$ [52, 53].

where $f(T)$ is a function of the temperature and d_{02}, d_{20}, d_{11} are constants [29]. We know that the conductivities have the same dimension as the temperature or chemical potentials, $[\sigma_5] = [\sigma_{5e}] = [T] = [\mu] = [\mu_5]$. So, if there are no extra dimensionful quantities in the model, it is valid to conclude that $f(T) \simeq T$, which also supports the general scaling behaviors as summarized in table 1.

On the universal scaling behaviors in the high temperature regime, for a physical explanation, it is nature to assume that the interaction between the charges in the fluid will become weaker in the higher temperature. The Ohmic conductivity σ_e describes the response of the charged vector current to the external electrical field, $\sigma_e \simeq \vec{J}/\vec{E}$. When the temperature is increased, σ_e will be enhanced because the moving of the charges in the fluid will become easier. However, the CESE conductivity σ_{5e} measures the response of the axial current to the external electrical field, $\sigma_{5e} \simeq \vec{J}_5/\vec{E}$. When temperature is increased, the interaction between the axial current and electrical field will become weaker and σ_{5e} will decrease due to the additional interaction factor $\left(\frac{\bar{\mu}}{T}\right)\left(\frac{\bar{\mu}_5}{T}\right)$.

While the CESE is a non-anomalous transport phenomenon, it may induce phenomenological consequences in heavy-ion collisions, namely the net charge distribution and correlation patterns in Cu+Au collisions as discussed in [28]. Admittedly, this should be a mixture due to CESE, CME, and CSE. However, CESE, along with other robust anomalous transport phenomena, is masked by various backgrounds in heavy-ion collisions, making it very difficult to pin down, not even to explore its properties. On the other hand, the exotic topological states of metal, such as Dirac and Weyl semi-metals, provide an experimental playground to study potential observable effects of CESE and other anomalous transports in a controllable way. See [27, 35–37] for recent progress on this topic, as well as the relevant investigations from holographic models [54–62].

Below we would like to rewrite the currents (1.3) and (1.4) in a linear response form, in which the electric field E_i and thermal gradient $\nabla_i T$ are taken as external sources. In other words, the fluid velocity u_i will be eliminated using the current conservation law

in (1.6). Here, the chemical potentials μ, μ_5 will be taken as constant. Consequently,

$$u^i = u_i = \frac{1}{i\omega}\left(s\nabla_i T - \frac{\rho}{\mathcal{E}+\mathcal{P}}E_i\right), \tag{1.14}$$

where $\partial_t \to -i\omega$ is used. Then, the currents (1.3) and (1.4) turn into

$$J^t = \rho, \qquad\qquad J_i = \sigma_{(\omega)}E_i - \alpha_{(\omega)}\nabla_i T, \tag{1.15}$$

$$J_5^t = \rho_5, \qquad\qquad J_{5i} = \sigma_{5(\omega)}E_i - \alpha_{5(\omega)}\nabla_i T, \tag{1.16}$$

where

$$\sigma_{(\omega)} = \frac{i}{\omega}\frac{\rho^2}{\mathcal{E}+\mathcal{P}} + \sigma_e, \qquad\qquad \sigma_{5(\omega)} = \frac{i}{\omega}\frac{\rho\rho_5}{\mathcal{E}+\mathcal{P}} + \sigma_{5e}, \tag{1.17}$$

$$\alpha_{(\omega)}T = \frac{i}{\omega}\rho - \left(\mu\,\sigma_{(\omega)} + \mu_5\,\sigma_{5(\omega)}\right), \qquad \alpha_{5(\omega)}T = \frac{i}{\omega}\rho_5 - \left(\mu_5\,\tilde{\sigma}_{(\omega)} + \mu\,\sigma_{5(\omega)}\right). \tag{1.18}$$

In (1.18), $\tilde{\sigma}_{(\omega)}$ is related to $\tilde{\sigma}_e$ by

$$\tilde{\sigma}_{(\omega)} \equiv \sigma_{(\omega)}\big|_{\rho\leftrightarrow\rho_5} = \frac{i}{\omega}\frac{\rho_5^2}{\mathcal{E}+\mathcal{P}} + \tilde{\sigma}_e, \tag{1.19}$$

where $\tilde{\sigma}_e$ is presented in (1.8). Physically, $\sigma_{(\omega)}$ is the low-frequency limit of the Ohmic electrical conductivity, and $\sigma_{5(\omega)}$ measures the chiral electrical separation effect. Obviously, in the probe limit, $\sigma_{(\omega)}$ and $\sigma_{5(\omega)}$ are dominated by their intrinsic parts σ_e and σ_{5e}. $\alpha_{(\omega)}$ and $\alpha_{5(\omega)}$ are the thermoelectric conductivities for vector and axial currents. The heat current is

$$\mathcal{Q}^i \equiv T^{ti} - \mu J^i - \mu_5 J_5^i = \bar{\alpha}_{(\omega)}TE_i - \bar{\kappa}_{(\omega)}\nabla_i T, \tag{1.20}$$

where the transport coefficients are

$$\bar{\alpha}_{(\omega)} = \alpha_{(\omega)}, \quad \bar{\kappa}_{(\omega)}T = \frac{i}{\omega}\left(\mathcal{E}+\mathcal{P}-2\rho\mu-2\rho_5\mu_5\right) + \left(\mu^2\,\sigma_{(\omega)} + \mu_5^2\,\tilde{\sigma}_{(\omega)} + 2\mu\mu_5\sigma_{5(\omega)}\right). \tag{1.21}$$

$\bar{\kappa}_{(\omega)}$ is the low-frequency limit of thermal conductivity, and it is fully determined by the intrinsic conductivities σ_e, σ_{5e} in (1.8). Here we would like to emphasize that $\sigma_{(\omega)}, \sigma_{5(\omega)}$, $\tilde{\sigma}_{(\omega)}, \alpha_{(\omega)}, \alpha_{5(\omega)}, \bar{\alpha}_{(\omega)}, \bar{\kappa}_{(\omega)}$ are different from the intrinsic conductivities $\sigma_e, \sigma_{5e}, \tilde{\sigma}_e, \tilde{\sigma}_{5e}$: while the former could be directly read off from associated Kubo formulas, the latter are useful in parameterizing the hydrodynamic constitutive relations (1.3)(1.4). In the probe limit, the differences between them are absent.

As the second study of the present work, we compute frequency-dependent conductivities. The external sources are vector and axial external fields E_i, E_i^5 and temperature gradient $\nabla_i T$, which depend on time via a plane waveform. As a result, the low-frequency conductivities $\sigma_{(\omega)}, \sigma_{5(\omega)}, \tilde{\sigma}_{(\omega)}, \alpha_{(\omega)}, \alpha_{5(\omega)}, \bar{\alpha}_{(\omega)}, \bar{\kappa}_{(\omega)}$ are generalized to frequency-dependent AC conductivities, see (4.13). First, we analytically evaluate the low-frequency limits of all the AC conductivities, demonstrating agreement with (1.17), (1.18), (1.19), (1.21). For the general value of frequency, we numerically compute all AC conductivities, see plots in section 4.

Note the appearance of i/ω pieces in the physical conductivities $\sigma_{(\omega)}$ and $\sigma_{5(\omega)}$. Via Kramers-Kronig relations [63, 64], this i/ω immediately implies the existence of a $\delta(\omega)$ in real parts of $\sigma_{(\omega)}$ and $\sigma_{5(\omega)}$, as is required by translation invariance. However, in holographic models with spatial translational symmetry, it is hard to reveal the delta peak in DC conductivity analytically. Once translational symmetry is broken, the DC conductivities become finite with the delta peak removed. Within the relaxation time approximation, the momentum dissipation effect would result in the replacement

$$\frac{i}{\omega} = \frac{1}{-i\omega} \;\rightarrow\; \frac{1}{1/\tau - i\omega}, \tag{1.22}$$

where τ corresponds to momentum relaxation time. Now all physical conductivities become finite and, in particular, they are split into two parts: the "coherent" pieces (related to the momentum dissipation) and the "inherent" ones (the universal pieces). Admittedly, a more rigorous treatment of momentum dissipation along the line [41–43, 65, 66] would be useful in clarifying physical meanings of these transport coefficients, and we will address this elsewhere.

The remaining sections are structured as follows. In section 2, we present the holographic model. In section 3, with anomalous terms neglected, we re-derive the first-order constitutive relations (1.1) (1.3) (1.4) using the fluid/gravity correspondence, and analytically compute all dissipative transport coefficients. In section 4, we obtain AC conductivities through linear response analysis. Section 5 contains the conclusion and discussions. Two appendices A and B provide further calculational details.

Notation conventions. We use the upper-case Latin letters $M, N, \cdots$ to denote the $(4 + 1)$-dimensional bulk coordinates, the lower-case Greek letters $\mu, \nu, \cdots$ to denote the $(3 + 1)$-dimensional boundary directions, while $i, j, \cdots$ will be used for spatial directions on the boundary.

2 Holographic model for fluid with $\mathrm{U}(1)_V \times \mathrm{U}(1)_A$ currents

We consider $(4 + 1)$-dimensional Einstein gravity with a negative cosmological constant $\Lambda = -6/L^2$ in the bulk, which is coupled to $\mathrm{U}(1)_V \times \mathrm{U}(1)_A$ gauge fields (see, e.g., [44, 45]). The total bulk action is

$$\mathcal{S}_{\mathcal{M}} = \frac{1}{16\pi G_5} \int_{\mathcal{M}} \mathrm{d}^5 x \sqrt{-g}\,(R - 2\Lambda) + \mathcal{S}_F + \mathcal{S}_{\mathrm{ct}} + \mathcal{S}_{\mathcal{K}}, \tag{2.1}$$

where

$$\mathcal{S}_F = -\int_{\mathcal{M}} \mathrm{d}^5 x \sqrt{-g}\,\left(\frac{1}{4q_V^2} F_{MN} F^{MN} + \frac{1}{4q_A^2} \tilde{F}_{MN} \tilde{F}^{MN}\right). \tag{2.2}$$

The field strengths of the bulk U(1) gauge fields are defined as $F_{MN} \equiv \partial_M A_N - \partial_N A_M$ and $\tilde{F}_{MN} \equiv \partial_M \tilde{A}_N - \partial_N \tilde{A}_M$. In our notations, A_M and $\tilde{A}_M$ denote the vector and axial bulk gauge fields, which are dual to vector and axial currents J^μ, J_5^μ of the boundary conformal field theory (CFT), respectively. The Gibbons-Hawking-York term $\mathcal{S}_{\mathcal{K}}$ is

$$\mathcal{S}_{\mathcal{K}} = \frac{1}{8\pi G_5} \int_{\partial\mathcal{M}} \mathrm{d}^4 x \sqrt{-\gamma}\,\mathcal{K}, \tag{2.3}$$

where $\mathcal{K} = \gamma^{\mu\nu} \mathcal{K}_{\mu\nu}$. $\gamma_{\mu\nu}$ is the induced metric on the boundary hypersurface Σ defined by the equation $r = r_c$, and $\mathcal{K}_{\mu\nu}$ is the extrinsic curvature tensor on Σ,

$$\mathcal{K}_{\mu\nu} = \frac{1}{2} \mathcal{L}_n \gamma_{\mu\nu} \equiv \frac{1}{2} \left(n^M \partial_M \gamma_{\mu\nu} + \gamma_{\mu N} \partial_\nu n^N + \gamma_{\nu N} \partial_\mu n^N \right), \qquad (2.4)$$

where $\mathcal{L}_n$ is the Lie derivative along the unit normal vector n_M of the hypersurface Σ:

$$n_M = \frac{\partial_M r}{\sqrt{g^{AB} \partial_A r \partial_B r}}. \qquad (2.5)$$

The counter-term action $\mathcal{S}_{\mathrm{ct}}$ is [53, 67–71]

$$\mathcal{S}_{\mathrm{ct}} = -\frac{1}{16\pi G_5} \int_{\partial\mathcal{M}} \mathrm{d}^4 x \sqrt{-\gamma} \left(\frac{1}{2} \mathcal{R} + 6 \right) + \frac{\log r_c}{4} \int_{\partial\mathcal{M}} \mathrm{d}^4 x \sqrt{-\gamma} \left(\frac{1}{q_V^2} F_{\mu\nu} F^{\mu\nu} + \frac{1}{q_A^2} \tilde{F}_{\mu\nu} \tilde{F}^{\mu\nu} \right), \qquad (2.6)$$

where $\mathcal{R}$ is the Ricci scalar of the induced metric $\gamma_{\mu\nu}$. Note minimal subtraction scheme has been utilized in writing down the counter-terms for bulk Maxwell fields. $F_{\mu\nu}$ and $\tilde{F}_{\mu\nu}$ in (2.6) are the projections of bulk field strengths F_{MN} and $\tilde{F}_{MN}$ onto the hypersurface Σ.

We would like to stress once again that the possible Chern-Simons terms $\tilde{A} \wedge F \wedge F$ and $\tilde{A} \wedge \tilde{F} \wedge \tilde{F}$ have been ignored in (2.1), which amounts to switching off the chiral anomaly effect in the dual boundary theory [44, 45]. Indeed, in order for the chiral anomaly to take effect, the dual plasma should either be exposed to a magnetic environment or rotate. Thus, with an electric field as the only external source, all the anomalous transports in (1.3)(1.4) vanish accidentally.

Variation of total bulk action $\mathcal{S}_\mathcal{M}$ in (2.1) with respect to bulk metric g_{MN} gives rise to the Einstein equation,

$$W_{MN} \equiv R_{MN} - \frac{1}{2} R\, g_{MN} - 6 g_{MN} - \left(T_{MN}^{\mathrm{bulk}} + \tilde{T}_{MN}^{\mathrm{bulk}} \right) = 0, \qquad (2.7)$$

where

$$T_{MN}^{\mathrm{bulk}} = \frac{q}{2} \left(F_{AM} F^A{}_N - \frac{1}{4} g_{MN} F^2 \right), \qquad q \equiv \frac{16\pi G_5}{q_V^2},$$

$$\tilde{T}_{MN}^{\mathrm{bulk}} = \frac{\tilde{q}}{2} \left(\tilde{F}_{AM} \tilde{F}^A{}_N - \frac{1}{4} g_{MN} \tilde{F}^2 \right), \qquad \tilde{q} \equiv \frac{16\pi G_5}{q_A^2}.$$

The bulk stress-energy tensor has been denoted as T_{MN}^{bulk} and $\tilde{T}_{MN}^{\mathrm{bulk}}$, which should not be confused with that of the dual boundary theory. q and $\tilde{q}$ measure the strength of back-reaction of bulk gauge fields on the bulk geometry. The Maxwell equations for A_M and $\tilde{A}_M$ are,

$$W^N \equiv \nabla_M F^{MN} = \frac{1}{\sqrt{-g}} \partial_M \left(\sqrt{-g} F^{MN} \right) = 0, \qquad (2.8)$$

$$\tilde{W}^N \equiv \nabla_M \tilde{F}^{MN} = \frac{1}{\sqrt{-g}} \partial_M \left(\sqrt{-g} \tilde{F}^{MN} \right) = 0. \qquad (2.9)$$

According to Anti-de Sitter/Conformal Field Theory (AdS/CFT) correspondence [72–74], the expectation values of stress-energy tensor and currents on the boundary theory are defined as

$$T_{\mu\nu} \equiv \lim_{r\to\infty} \frac{-2r^2}{\sqrt{-\gamma}} \frac{\delta S_{\mathcal{M}}}{\delta\gamma^{\mu\nu}}, \qquad J^\mu \equiv \lim_{r\to\infty} \frac{\delta S_{\mathcal{M}}}{\delta A_\mu}, \qquad J_5^\mu \equiv \lim_{r\to\infty} \frac{\delta S_{\mathcal{M}}}{\delta\tilde{A}_\mu}. \tag{2.10}$$

In terms of bulk fields, (2.10) turns into

$$T_{\mu\nu} = -\frac{1}{8\pi G_5} \lim_{r\to\infty} r^2 \left[\left(\mathcal{K}_{\mu\nu} - \mathcal{K}\gamma_{\mu\nu} + 3\gamma_{\mu\nu} - \frac{1}{2}\mathcal{G}_{\mu\nu} \right) + \mathcal{T}_{\mu\nu}^F \right], \tag{2.11}$$

$$J^\mu = -\frac{1}{q_V^2} \lim_{r\to\infty} r^2 \left(n_M F^{M\mu} + D_\nu F^{\nu\mu} \log r \right), \tag{2.12}$$

$$J_5^\mu = -\frac{1}{q_A^2} \lim_{r\to\infty} r^2 \left(n_M \tilde{F}^{M\mu} + D_\nu \tilde{F}^{\nu\mu} \log r \right), \tag{2.13}$$

where the counter-term

$$\mathcal{T}_{\mu\nu}^F \equiv \frac{\log r}{4q_V^2} \left(F_{\alpha\mu}F^\alpha{}_\nu - \frac{1}{4}\gamma_{\mu\nu}F^2 \right) + \frac{\log r}{4q_A^2} \left(\tilde{F}_{\alpha\mu}\tilde{F}^\alpha{}_\nu - \frac{1}{4}\gamma_{\mu\nu}\tilde{F}^2 \right), \tag{2.14}$$

which will affect the study of section 4 beyond first-order transport coefficients. In (2.11)–(2.13), $\mathcal{G}_{\mu\nu}$ is the Einstein tensor associated with the induced metric $\gamma_{\mu\nu}$, and D is the covariant derivative operator compatible with $\gamma_{\mu\nu}$.

The bulk equations (2.7)–(2.9) can be classified into dynamical components and constraint ones. Moreover, the constraint components correspond to conservation laws for boundary stress-energy tensor and currents:

$$\begin{aligned}
W^r{}_\nu = 0 &\Rightarrow \partial^\mu T_{\mu\nu} = J^\alpha F_{\nu\alpha}^{(\epsilon)} + J_5^\alpha \tilde{F}_{\nu\alpha}^{(\epsilon)}, \\
W^r = 0 &\Rightarrow \partial_\mu J^\mu = 0, \\
\tilde{W}^r = 0 &\Rightarrow \partial_\mu J_5^\mu = 0,
\end{aligned} \tag{2.15}$$

where $F_{\nu\alpha}^{(\epsilon)}$ and $\tilde{F}_{\nu\alpha}^{(\epsilon)}$ are external vector and axial electromagnetic field strengths, respectively.

In what follows, we will work under the convention $16\pi G_5 = 1$ and $L = 1$. The bulk gauge couplings q_V, q_A will be absorbed into redefinitions of bulk gauge fields $A_M \to q_V A_M$ and $\tilde{A}_M \to q_A \tilde{A}_M$. The boundary CFT in thermal equilibrium corresponds to a homogeneous solution of the bulk theory (2.1). We assume the presence of finite vector and axial charge densities. Consequently, the homogeneous solution of the bulk theory is the AdS$_5$ black brane with two charges,

$$\begin{aligned}
ds_{(0)}^2 &= g_{MN}^{(0)} dx^M dx^N = 2dtdr - r^2 f(r)dt^2 + r^2 \delta_{ij} dx^i dx^j, \\
f(r) &\equiv 1 - \frac{M}{r^4} + \frac{Q^2 + \tilde{Q}^2}{r^6} = \frac{\left(r^2 - r_h^2\right)\left(r^2 - r_-^2\right)\left(r^2 + r_h^2 + r_-^2\right)}{r^6}, \\
A_{(0)} &= -\frac{\sqrt{3}Q}{r^2}dt, \qquad \tilde{A}_{(0)} = -\frac{\sqrt{3}\tilde{Q}}{r^2}dt,
\end{aligned} \tag{2.16}$$

where $M, Q, \tilde{Q}$ are constant parameters of the bulk theory.

In (2.16), r_h is the largest root for $f(r) = 0$, defining the location of event horizon of the two-charges AdS$_5$ black brane. The Hawking temperature, identified as the temperature of dual boundary field theory, is

$$T_0 = \frac{\partial_r \left(r^2 f(r) \right)}{4\pi} \bigg|_{r=r_h} = \frac{r_h}{\pi} \left(1 - \frac{Q^2 + \tilde{Q}^2}{2r_h^6} \right), \tag{2.17}$$

which should be non-negative, setting constraints on the combination $(Q^2 + \tilde{Q}^2)$. At the horizon with a constant time section, the line element degenerates into $ds^2|_{\text{Horizon}} = r_h^2 \delta_{ij} \mathrm{d}x^i \mathrm{d}x^j$, with $i, j = 1, 2, 3$. Thus, the entropy density of the black brane (2.16), which will be identified as that of the dual CFT, turns out to be

$$s_0 = \frac{\text{Area}(r_h)}{4G_5} = \frac{r_h^3}{4G_5} = 4\pi r_h^3, \tag{2.18}$$

where in the second equality we made use of the normalization convention $16\pi G_5 = 1$. The subscript "$_0$" in (2.17) (2.18) is to emphasize that they are constant, as compared to temperature field $T(x^\alpha)$ in section 3.

Finally, via (2.11)–(2.13), the dual stress-energy tensor and currents of the boundary theory are

$$T_{(0)}^{\mu\nu} = 3M \, \delta_t^\mu \delta_t^\nu + M \, \delta_i^\mu \delta_j^\nu, \qquad J_{(0)}^\mu = 2\sqrt{3}Q \, \delta_t^\mu, \qquad J_{5(0)}^\mu = 2\sqrt{3}\tilde{Q} \, \delta_t^\mu, \tag{2.19}$$

where the subscript "$_{(0)}$" is to mark that these quantities are associated to a state in thermal equilibrium. If we make the following identifications,

$$\mathcal{E} = 3M, \qquad \mathcal{P} = M, \qquad \rho = 2\sqrt{3}Q, \qquad \rho_5 = 2\sqrt{3}\tilde{Q}, \tag{2.20}$$

then (2.19) are nothing but the non-derivative parts of the stress-energy tensor and currents (1.1) (1.3) (1.4) in local rest frame where $u_\mu = (-1, 0, 0, 0)$. In the next two sections 3 and 4 we will solve the bulk dynamics with equations of motion (2.7) (2.8) (2.9) under two complementary limits, hydrodynamic limit versus linear approximation, generating viscous corrections to ideal fluid (2.19).

3 First order hydrodynamics from fluid/gravity correspondence

In this section, we construct the first-order hydrodynamics dual to the bulk theory (2.1) via the fluid/gravity correspondence [47, 75].

3.1 Set up the fluid/gravity calculations

In this subsection, we set up the stage for performing fluid/gravity calculations for the bulk theory of (2.1). Following the standard procedure of fluid/gravity correspondence [47, 75], we make a Lorenz boost transformation for the static solution (2.16) along the boundary coordinates

$$x^\mu \to L^\mu{}_\nu x^\nu, \qquad L^t{}_\nu = -u_\nu, \qquad L^i{}_\nu = \left(-u^i, \delta_j^i + \frac{u^i u_j}{1 - u_0} \right). \tag{3.1}$$

$L^\mu{}_\nu$ is the Lorentz boost matrix, which has been parameterized via a four-velocity u_μ. Note the four-velocity u_μ is a time-like unit vector obeying $\eta^{\mu\nu} u_\mu u_\nu = -1$, which leads to $u_0 = -\sqrt{1 + \vec{u}^2}$. After the transformation (3.1), the homogenous solution (2.16) turns into

$$ds^2_{(u)} = -r^2 f(r)(u_\mu dx^\mu)^2 - 2u_\mu dx^\mu dr + r^2(\eta_{\mu\nu} + u_\mu u_\nu)dx^\mu dx^\nu,$$

$$A_{(u)} = \frac{\sqrt{3}Q}{r^2} u_\mu dx^\mu + A^{(\epsilon)}_\mu dx^\mu, \qquad \tilde{A}_{(u)} = \frac{\sqrt{3}\tilde{Q}}{r^2} u_\mu dx^\mu, \tag{3.2}$$

$$f(r) = 1 - \frac{M}{r^4} + \frac{Q^2 + \tilde{Q}^2}{r^6},$$

where a constant vector field $A^{(\epsilon)}_\mu$ is introduced for the later purpose of exposing the boundary theory to an external electric field environment. So long as the parameters $M, Q, \tilde{Q}, A^{(\epsilon)}_\mu$ are constants, the boosted solution (3.2) does solve the bulk equations of motion (2.7)–(2.9).

One key procedure of fluid/gravity correspondence is to promote the constant parameters in (3.2) to arbitrary functions of boundary coordinates [7, 47, 75, 76],

$$M \to M(x^\alpha), \quad Q \to Q(x^\alpha), \quad \tilde{Q} \to \tilde{Q}(x^\alpha), \quad u_\mu \to u_\mu(x^\alpha), \quad A^{(\epsilon)}_\mu \to A^{(\epsilon)}_\mu(x^\alpha). \tag{3.3}$$

Then, these nontrivial functions $M(x), Q(x), \tilde{Q}(x), u_\mu(x)$ and $A^{(\epsilon)}_\mu(x)$ are identified as the fluid-dynamical variables and external source of the dual field theory. However, after the promotion (3.3) the boosted solution (3.2) will not satisfy the bulk equations (2.7)–(2.9) any more. That is, the price of the promotion (3.3) is that one has to add suitable corrections to the metric and gauge fields in the bulk theory so that the bulk equations (2.7)–(2.9) can be obeyed. For general functions $M(x), Q(x), \tilde{Q}(x), u_\mu(x)$ and $A^{(\epsilon)}_\mu(x)$, it is very difficult to work out these suitable corrections. The fluid/gravity correspondence shows that in the hydrodynamic limit, where the functions $M(x), Q(x), \tilde{Q}(x), u_\mu(x)$ and $A^{(\epsilon)}_\mu(x)$ vary rather slowly from point to point, the corrections can be systematically collected order-by-order within a boundary derivative expansion.

In the practical calculation, we do Taylor expansion for $M(x), Q(x), \tilde{Q}(x), u_\mu(x)$ and $A^{(\epsilon)}_\mu(x)$ around the point of origin $x^\mu = 0$,

$$\begin{aligned} M(x) &= M_0 + \varepsilon x^\alpha \partial_\alpha M + O(\partial^2), & u_\mu(x) &= (-1, \varepsilon(x^\alpha \partial_\alpha u_i)) + O(\partial^2), \\ Q(x) &= Q_0 + \varepsilon x^\alpha \partial_\alpha Q + O(\partial^2), & \tilde{Q}(x) &= \tilde{Q}_0 + \varepsilon x^\alpha \partial_\alpha \tilde{Q} + O(\partial^2), \\ A^{(\epsilon)}_\mu(x) &= 0 + \varepsilon x^\alpha \partial_\alpha A^{(\epsilon)}_\mu + O(\partial^2), \end{aligned} \tag{3.4}$$

where we have chosen the frame that $u_i = 0$ and $A^{(\epsilon)}_\mu = 0$ at the origin. Moreover, a formal parameter ε is introduced to count the number of derivatives in the expansion, and eventually will be set to unity. All calculations in this section will be accurate up to the first-order in the derivative expansion. Consequently, up to order $\mathcal{O}(\varepsilon^1)$ the promoted

metric and gauge fields become

$$ds^2_{(u)} = g^{(u)}_{MN} dx^M dx^N = 2dtdr - r^2 f_0(r)dt^2 + r^2 \delta_{ij} dx^i dx^j$$
$$- \varepsilon \left\{ r^2 f_1(r,x)dt^2 - 2r^2[f_0(r)-1](x^\alpha \partial_\alpha u_i)dtdx^i + 2(x^\alpha \partial_\alpha u_i)dx^i dr \right\},$$

$$A^{(u)} = A^{(u)}_M dx^M = -\frac{\sqrt{3}(Q_0 + x^\alpha \partial_\alpha Q)}{r^2}dt + \varepsilon \frac{\sqrt{3}Q_0}{r^2}(x^\alpha \partial_\alpha u_i)dx^i + x^\alpha \partial_\alpha A^{(\epsilon)}_\mu dx^\mu,$$

$$\tilde{A}^{(u)} = \tilde{A}^{(u)}_M dx^M = -\frac{\sqrt{3}(\tilde{Q}_0 + x^\alpha \partial_\alpha \tilde{Q})}{r^2}dt + \varepsilon \frac{\sqrt{3}\tilde{Q}_0}{r^2}(x^\alpha \partial_\alpha u_i)dx^i, \tag{3.5}$$

where

$$f_0(r) = 1 - \frac{M_0}{r^4} + \frac{Q_0^2 + \tilde{Q}_0^2}{r^6}, \qquad f_1(r,x) = -\frac{x^\alpha \partial_\alpha M}{r^4} + \frac{2Q_0 x^\alpha \partial_\alpha Q + 2\tilde{Q}_0 x^\alpha \partial_\alpha \tilde{Q}}{r^6}. \tag{3.6}$$

As explained below (3.3), in order to satisfy the equations of motion (2.7)–(2.9), suitable corrections must be added on top of (3.5). Up to the first-order in the derivative expansion,

$$ds^2_{(1)} \equiv g^{(1)}_{MN} dx^M dx^N = \frac{k(r)}{r^2}dt^2 + 2h(r)dtdr + \frac{2j_i(r)}{r^2}dtdx^i + r^2 \left[\alpha_{ij}(r) - \frac{2}{3}\delta_{ij}h(r) \right] dx^i dx^j,$$

$$A^{(1)} = A^{(1)}_M dx^M = a_t(r)dt + a_i(r)dx^i, \qquad \tilde{A}^{(1)} = \tilde{A}^{(1)}_M dx^M = \tilde{a}_t(r)dt + \tilde{a}_i(r)dx^i, \tag{3.7}$$

where $\alpha_{ij}(r)$ is a traceless symmetric tensor of rank two under SO(3) rotational symmetry between the spatial directions x^i. In the parameterizing of the corrections (3.7), we choose the following gauge convention

$$g^{(1)}_{rr} = 0, \qquad g^{(1)}_{r\mu} \propto u_\mu, \qquad \text{Tr}\left[(g^{\text{eq}})^{-1} g^{(1)} \right] = 0, \qquad A^{(1)}_r = \tilde{A}^{(1)}_r = 0. \tag{3.8}$$

Plugging the total bulk metric and gauge fields

$$g_{MN} = g^{(u)}_{MN} + g^{(1)}_{MN}, \qquad A_M = A^{(u)}_M + A^{(1)}_M, \qquad \tilde{A}_M = \tilde{A}^{(u)}_M + \tilde{A}^{(1)}_M, \tag{3.9}$$

into (2.7)–(2.9) results in a system of ordinary differential equations for those corrections in (3.7). We need to specify suitable boundary conditions in order to fully determine the corrections. The first type of boundary condition is the requirement of asymptotic AdS, which fixes the large r behavior for the corrections,

$$\begin{aligned} k(r) < O(r^4), &\qquad h(r) < O(r^0), &\qquad j_i(r) < O(r^4), &\qquad \alpha_{ij}(r) < O(r^0), \\ a_t(r) < O(r^0), &\qquad \tilde{a}_t(r) < O(r^0), &\qquad a_i(r) < O(r^0), &\qquad \tilde{a}_i(r) < O(r^0). \end{aligned} \tag{3.10}$$

The second type of boundary condition is the regularity requirement for all the corrections in (3.7),

$$h(r), \, k(r), \, j_i(r), \, \alpha_{ij}(r), \, a_t(r), \, a_i(r), \, \tilde{a}_t(r), \, \tilde{a}_i(r) \text{ are regular over } r \in [r_h, +\infty), \tag{3.11}$$

which turns out to be effective at the event horizon $r = r_h$. The remaining ambiguity of determining the corrections of (3.7) will be fixed by the frame convention. We will work in Landau-Lifshitz frame so that

$$u_\mu T^{\mu\nu} = -\mathcal{E}u^\nu, \qquad u_\mu J^\mu = -\rho, \qquad u_\mu J^\mu_5 = -\rho_5, \tag{3.12}$$

– 14 –

where $\mathcal{E}$, ρ, ρ_5 are the energy density, vector and axial charge densities of the fluid, respectively,

$$\mathcal{E} = 3M(x), \qquad \rho = 2\sqrt{3}Q(x), \qquad \rho_5 = 2\sqrt{3}\tilde{Q}(x). \qquad (3.13)$$

Note the identification made in (3.13) is the promotion from their in-equilibrium counterparts (2.20). Up to the first-order in the derivative expansion, the Landau-Lifshitz frame conditions (3.12) turn into constraints on the form of boundary stress-energy tensor and currents,

$$T_{tt} = 3M_0 + 3x^\alpha \partial_\alpha M, \qquad T_{ti} = T_{it} = -4M_0(x^\alpha \partial_\alpha u_i), \qquad (3.14)$$

$$J^t = 2\sqrt{3}\left[Q_0 + x^\alpha \partial_\alpha Q\right], \qquad J_5^t = 2\sqrt{3}\left[\tilde{Q}_0 + x^\alpha \partial_\alpha \tilde{Q}\right]. \qquad (3.15)$$

For the sake of later presentation, we rewrite the expressions (2.11)–(2.13) in terms of those corrections in (3.7),

$$T_{tt} = 3M_0 + 3x^\mu \partial_\mu M - 2r^3(\partial_k u_k) + 6r^4 h(r) + 2r^5 \partial_r h(r) + 3k(r), \qquad (3.16)$$

$$T_{ti} = T_{it} = -r^3 \partial_t u_i + 4j_i(r) - r\partial_r j_i(r) - 4M_0(x^\alpha \partial_\alpha u_i), \qquad (3.17)$$

$$T_{ij} = \left[M_0 + x^\alpha \partial_\alpha M + k(r) - r\partial_r k(r) - 6r^4 h(r) + \frac{4}{3}r^3(\partial_k u_k)\right]\delta_{ij}$$
$$- r^3\left[\partial_i u_j + \partial_j u_i - \frac{2}{3}\delta_{ij}(\partial_k u_k)\right] - r^5 \partial_r \alpha_{ij}(r), \qquad (3.18)$$

as well as

$$J^t = 2\sqrt{3}(Q_0 + x^\alpha \partial_\alpha Q) + r^3 \partial_r a_t, \quad J^i = 2\sqrt{3}Q_0(x^\alpha \partial_\alpha u_i) - r^3 \partial_r a_i(r) - rF_{ti}^{(\epsilon)}, \qquad (3.19)$$

$$J_5^t = 2\sqrt{3}(\tilde{Q}_0 + x^\alpha \partial_\alpha \tilde{Q}) + r^3 \partial_r \tilde{a}_t, \quad J_5^i = 2\sqrt{3}\tilde{Q}_0(x^\alpha \partial_\alpha u_i) - r^3 \partial_r \tilde{a}_i(r). \qquad (3.20)$$

The limit of $r \to \infty$ is assumed implicitly in expressions above (3.16)–(3.20), and we have also ignored the terms that will be explicitly vanishing as $r \to \infty$.

While the bulk corrections will be constructed around $x^\mu = 0$, they do contain enough information to write down the total bulk metric and gauge fields about any point, valid up to the first-order in the derivative expansion. Instead of following this approach of [47], we will compute the boundary stress-energy tensor and currents using thus-constructed solutions, via the formulas (3.16)–(3.20). Eventually, we will lift up thus-obtained constitutive relations into a covariant form.

3.2 First-order charged fluid: CESE and other conductivities

Following section 3.1, it is straightforward to solve the bulk equations (2.7)–(2.9) and obtain the corrections in (3.7). In what follows, we summarize the final results and leave all the calculation details in appendix A.1. We present by grouping them into different sectors under SO(3) symmetry of the boundary spatial directions.

In the scalar sector,

$$k(r) = \frac{2}{3}r^3(\partial_k u_k), \qquad h(r) = 0, \qquad a_t(r) = 0, \qquad \tilde{a}_t(r) = 0. \qquad (3.21)$$

In the vector sector, thanks to going beyond the probe limit, dynamical equations for $j_i, a_i, \tilde{a}_i$ are coupled, see (A.13)–(A.15). It is exactly this coupling that makes CESE non-vanish, as opposed to the probe limit [45, 46]. Since the final solutions in the vector sector are very lengthy, we record their near boundary expansions only,

$$a_i(r) \xrightarrow{r \to \infty} -\frac{3\sqrt{3}Q_0}{r^2}\left(\frac{r_h^3}{4M_0} + \frac{1}{4r_h}\right)\partial_t u_i - \frac{\sqrt{3}}{r^2}\frac{(2r_h^6 + Q_0^2 + 2\tilde{Q}_0^2)}{4M_0 r_h^3}\partial_i Q + \frac{\sqrt{3}}{r^2}\frac{Q_0\tilde{Q}_0}{4M_0 r_h^3}\partial_i\tilde{Q}$$

$$+ \frac{1}{r}F_{ti}^{(\epsilon)} - \frac{1}{r^2}\left(\frac{3Q_0^2}{4M_0 r_h} + \frac{1}{2}r_h\right)F_{ti}^{(\epsilon)} + O\left(r^{-3}\right), \tag{3.22}$$

$$\tilde{a}_i(r) \xrightarrow{r \to \infty} -\frac{3\sqrt{3}\tilde{Q}_0}{r^2}\left(\frac{r_h^3}{4M_0} + \frac{1}{4r_h}\right)\partial_t u_i - \frac{\sqrt{3}}{r^2}\frac{(2r_h^6 + 2Q_0^2 + \tilde{Q}_0^2)}{4M_0 r_h^3}\partial_i\tilde{Q} + \frac{\sqrt{3}}{r^2}\frac{Q_0\tilde{Q}_0}{4M_0 r_h^3}\partial_i Q$$

$$- \frac{1}{r^2}\frac{3Q_0\tilde{Q}_0}{4M_0 r_h}F_{ti}^{(\epsilon)} + O\left(r^{-3}\right), \tag{3.23}$$

$$j_i(r) \xrightarrow{r \to \infty} r^3\partial_t u_i + O(r^{-1}). \tag{3.24}$$

The tensor sector is the most simple one

$$\alpha_{ij}(r) = 3\left[\partial_i u_j + \partial_j u_i - \frac{2}{3}\delta_{ij}(\partial_k u_k)\right]\int_\infty^r \frac{\mathrm{d}\hat{x}}{\hat{x}^5 f_0(\hat{x})}\int_{r_h}^{\hat{x}} y^2 \mathrm{d}y,$$

$$\xrightarrow{r \to \infty} \left(\frac{1}{r} - \frac{r_h^3}{4r^4}\right)\left[\partial_i u_j + \partial_j u_i - \frac{2}{3}\delta_{ij}(\partial_k u_k)\right] + O(r^{-5}). \tag{3.25}$$

Now it is direct to compute the boundary stress-energy tensor and currents by substituting (3.21)–(3.25) into (3.16)–(3.20). Once lifted up into covariant form, the boundary stress-energy tensor $T_{\mu\nu}$ is given by (1.1)(1.2)

$$T_{\mu\nu} = \mathcal{E}u_\mu u_\nu + \mathcal{P}P_{\mu\nu} - 2\eta\sigma_{\mu\nu} - \zeta(\partial_\alpha u^\alpha)P_{\mu\nu} + \cdots, \tag{3.26}$$

where the projection tensor $P_{\mu\nu}$ and shear tensor $\sigma_{\mu\nu}$ are defined as

$$P_{\mu\nu} = \eta_{\mu\nu} + u_\mu u_\nu, \qquad \sigma_{\mu\nu} \equiv \frac{1}{2}P_\mu^\alpha P_\nu^\beta\left(\partial_\alpha u_\beta + \partial_\beta u_\alpha\right) - \frac{1}{3}P_{\mu\nu}(\partial_\alpha u^\alpha). \tag{3.27}$$

$\mathcal{E}$ is the energy density and $\mathcal{P}$ is the pressure of the fluid, which satisfy $\mathcal{E} = 3\mathcal{P}$ and

$$\mathcal{E} = 3M(x), \qquad \mathcal{P} = M(x). \tag{3.28}$$

The shear viscosity η and bulk viscosity ζ are,

$$\eta = r_h(x)^3, \qquad \zeta = 0. \tag{3.29}$$

From (2.18), entropy density of the dual fluid is $s = 4\pi r_h(x)^3$. So, as expected, our result for shear viscosity η saturates the Kovtun-Son-Starinets (KSS) bound [77–79].

Plugging (3.21)–(3.23) into (3.19)–(3.20) generates boundary currents (A.27)–(A.29), which are, however, parameterized in terms of bulk quantities $Q(x), \tilde{Q}(x), r_h(x), M(x)$. Physically, we have to re-parameterize (A.27)–(A.29) via boundary fluid-dynamical variables. Moreover, the chemical potentials will be preferred in expressing the diffusive terms

of J^μ, J_5^μ. In what follows we outline the strategy of implementing this transformation but defer technical details to appendix A.2.

The vector and axial charge densities are promoted versions of (2.20):

$$\rho(x) = 2\sqrt{3}Q(x), \qquad \rho_5(x) = 2\sqrt{3}\tilde{Q}(x). \tag{3.30}$$

In the fluid/gravity correspondence, chemical potentials are defined as

$$\begin{aligned}
\mu(x) &\equiv A_t|_{r=\infty} - A_t|_{r=r_h(x)} = \frac{\sqrt{3}Q(x)}{r_h(x)^2}, \\
\mu_5(x) &\equiv \tilde{A}_t|_{r=\infty} - \tilde{A}_t|_{r=r_h(x)} = \frac{\sqrt{3}\tilde{Q}(x)}{r_h(x)^2}.
\end{aligned} \tag{3.31}$$

From (2.17), the temperature field of the dual fluid is

$$T = \frac{r_h(x)}{\pi}\left(1 - \frac{Q(x)^2 + \tilde{Q}(x)^2}{2r_h(x)^6}\right). \tag{3.32}$$

Using (3.28), (3.30)–(3.32), one can check that the following relation still holds

$$\mathcal{E} + \mathcal{P} = Ts + \mu\rho + \mu_5\rho_5. \tag{3.33}$$

The relations (3.31)–(3.32) are useful in expressing $\partial_i Q$, $\partial_i \tilde{Q}$ and $\partial_i r_h$ in terms of $\partial_i T/T$, $\partial_i \mu$ and $\partial_i \mu_5$, see (A.33)–(A.35) in appendix A.2. Eventually, (A.27)–(A.29) could be recast into covariant forms, which cover non-anomalous part of (1.3)(1.4) with all transport coefficients expressed in terms of bulk parameters

$$\sigma_e = r_h + \frac{3Q^2}{2Mr_h} - \frac{9Q^2}{2M}\left(\frac{r_h^3}{2M} + \frac{1}{2r_h}\right), \qquad \tilde{\sigma}_e = \sigma_e\big|_{Q\leftrightarrow\tilde{Q}}, \tag{3.34}$$

$$\sigma_{5e} = \frac{3Q\tilde{Q}}{2Mr_h} - \frac{9Q\tilde{Q}}{2M}\left(\frac{r_h^3}{2M} + \frac{1}{2r_h}\right), \qquad \tilde{\sigma}_{5e} = \sigma_{5e}. \tag{3.35}$$

Note independent transport coefficients are σ_e and σ_{5e}, which are "quantum critical" or "incoherent" conductivities of hydrodynamics as in [48–50]. This is partly due to the time-reversal symmetry of our holographic model.

Physically, bulk quantities in (3.34)(3.35) should be eliminated in favor of thermodynamic variables of the boundary fluid. There are several ways of presenting the results. When discussing single charge limit or probe limit, we find it more transparent to split the conductivities (3.34)(3.35) into two parts, represented by σ_Q and σ_0, as flashed in (1.8)(1.9). On the other hand, in comparison with relevant works [28–31], we express σ_e and σ_{5e} as functions of chemical potentials μ, μ_5 and fluid temperature T, as summarized in (1.11). We also recast the hydrodynamic constitutive relations (1.3)(1.4) into linear response form, see (1.15)(1.16). Then, we give a clarification for the differences between physical conductivities directly read off from Kubo formulas and intrinsic ones parameterizing hydrodynamic constitutive relations.

4 Holographic AC conductivities from linear response analysis

As a complementary study of section 3, in this section, we reveal some transport phenomena of the holographic model (2.1) through linear response analysis. We focus on the vector and axial currents generated by the external vector and axial electric fields and thermal gradient. We assume these external sources are weak in amplitudes and oscillate in time only.

4.1 Black brane fluctuations and conductivity matrix

To study linear response transports within the holographic framework, we follow standard procedure and perturb the homogeneous black brane (2.16)

$$g_{MN} = g_{MN}^{(0)} + \delta g_{MN}, \qquad A_M = A_M^{(0)} + \delta A_M, \qquad \tilde{A}_M = \tilde{A}_M^{(0)} + \delta \tilde{A}_M. \tag{4.1}$$

Diffeomorphism and U(1) gauge invariance in the bulk theory allow choosing a particular gauge. Different from (3.8), throughout this section, we will work under radial gauge convention,

$$\delta g_{rA} = 0, \qquad \delta A_r = 0, \qquad \delta \tilde{A}_r = 0. \tag{4.2}$$

Black brane fluctuations (4.1) could be classified into decoupled sectors [80] according to their transformation properties under the remaining symmetry group SO(3). For the purpose of computing electrical and thermal conductivities, we consider the helicity one sector only

$$\delta(ds^2) = \epsilon \, 2\delta g_{ti}(r,t) dt \mathrm{d}x^i, \qquad \delta A = \epsilon \, \delta A_i(r,t) \mathrm{d}x^i, \qquad \delta \tilde{A} = \epsilon \, \delta \tilde{A}_i(r,t) \mathrm{d}x^i, \tag{4.3}$$

where ϵ is a formal parameter marking the linearization. The calculations below will be accurate up to $\mathcal{O}(\epsilon^1)$, as required for linear response study.

Fluctuations (4.3) satisfy a system of partial differential equations, whose derivation is presented in appendix B, see (B.8)–(B.12). While there is no explicit interaction term between A and $\tilde{A}$ in the bulk action (2.1), fluctuations δA_i and $\delta \tilde{A}_i$ do interact via δg_{ti}. As in section 3, this is exactly our point that the CESE can be realized by going beyond probe limit in a simple holographic model.

We proceed by deriving the compact forms of stress-energy tensor and currents of the boundary theory. To this end, we solve (B.8)–(B.11) near conformal boundary $r = \infty$,

$$\delta g_{ti}(r,t) \xrightarrow{r \to \infty} r^2 \delta h_{ti}^{(0)}(t) + \frac{\delta h_{ti}^{(4)}(t)}{r^2} + O\left(r^{-3}\right), \tag{4.4}$$

$$\delta A_i(r,t) \xrightarrow{r \to \infty} \delta a_i^{(0)}(t) + \frac{\partial_t \delta a_i^{(0)}(t)}{r} + \frac{\delta a_i^{(2)}(t)}{r^2} - \frac{\log r}{2r^2} \partial_t^2 \delta a_i^{(0)}(t) + O\left(\frac{\log r}{r^3}\right), \tag{4.5}$$

$$\delta \tilde{A}_i(r,t) \xrightarrow{r \to \infty} \delta \tilde{a}_i^{(0)}(t) + \frac{\partial_t \delta \tilde{a}_i^{(0)}(t)}{r} + \frac{\delta \tilde{a}_i^{(2)}(t)}{r^2} - \frac{\log r}{2r^2} \partial_t^2 \delta \tilde{a}_i^{(0)}(t) + O\left(\frac{\log r}{r^3}\right), \tag{4.6}$$

where the non-normalizable modes $\delta h_{ti}^{(0)}(t)$, $\delta a_i^{(0)}(t)$, $\delta \tilde{a}_i^{(0)}(t)$ correspond to external sources, see (B.4)–(B.6) for the precise identification. The constraint equation (B.12) yields

$$4\delta h_{ti}^{(4)} = 2\sqrt{3} \left(\tilde{Q} \delta \tilde{a}_i^{(0)} + Q \delta a_i^{(0)} \right). \tag{4.7}$$

The rest normalizable modes $\delta a_i^{(2)}$, $\delta \tilde{a}_i^{(2)}$ have to be determined via fully solving the bulk equations (B.8)–(B.11). Our strategy of solving them goes in two steps: (1) factorize out the time-dependence by basis decomposition (B.18); (2) solve ordinary differential equations satisfied by decomposition coefficients, see (B.19)(B.20). As a result,

$$\delta a_i^{(2)} = \frac{\mu s_1 + \mu_5 s_2}{\mu^2 + \mu_5^2} \left(\mu \delta a_i^{(0)} + \mu_5 \delta \tilde{a}_i^{(0)} \right), \quad \delta \tilde{a}_i^{(2)} = \frac{\mu_5 s_1 - \mu s_2}{\mu^2 + \mu_5^2} \left(\mu \delta a_i^{(0)} + \mu_5 \delta \tilde{a}_i^{(0)} \right), \quad (4.8)$$

where s_1, s_2 encode pre-asymptotic behaviors of the decomposition coefficients, see (B.21).

With the near boundary expansions (4.4)–(4.6), the dual stress-energy tensor and currents (2.11)–(2.13) become,

$$T_{tt} = 3M, \qquad T_{ij} = M\delta_{ij}, \qquad T_{ti} = M\delta h_{ti}^{(0)} + 2\sqrt{3}(\tilde{Q}\delta \tilde{a}_i^{(0)} + Q\delta a_i^{(0)}), \qquad (4.9)$$

$$J^t = 2\sqrt{3}Q, \qquad J^i = 2\delta a_i^{(2)} - \frac{1}{2}\partial_t^2 \delta a_i^{(0)} - 2\sqrt{3}Q\delta h_{ti}^{(0)}, \qquad (4.10)$$

$$J_5^t = 2\sqrt{3}\tilde{Q}, \qquad J_5^i = 2\delta \tilde{a}_i^{(2)} - \frac{1}{2}\partial_t^2 \delta \tilde{a}_i^{(0)} - 2\sqrt{3}\tilde{Q}\delta h_{ti}^{(0)}, \qquad (4.11)$$

where the constraint relation (4.7) has been used to simplify T_{ti}. The heat current $\mathcal{Q}^i$ is defined as

$$\mathcal{Q}^i = T^{ti} - \mu J^i - \mu_5 J_5^i, \qquad (4.12)$$

where T^{ti} could be computed from T_{ti} by a weakly curved boundary metric $\eta_{\mu\nu} + \delta h_{ti}^{(0)}$. Thus, the currents (4.10)–(4.12), as the linear response to external sources $E_i, E_i^5, \nabla_i T$, can be summarized in a compact matrix form

$$\begin{pmatrix} J^i \\ J_5^i \\ \mathcal{Q}^i \end{pmatrix} = \begin{pmatrix} \sigma & \tilde{\sigma}_5 & \alpha T \\ \sigma_5 & \tilde{\sigma} & \alpha_5 T \\ \bar{\alpha}T & \bar{\alpha}_5 T & \bar{\kappa}T \end{pmatrix} \begin{pmatrix} E_i \\ E_i^5 \\ -\frac{\nabla_i T}{T} \end{pmatrix}, \qquad (4.13)$$

where (B.4)–(B.6) have been used.

The electrical conductivities are

$$\sigma = -\left[\underline{\pi\delta(\omega)} + \frac{i}{\omega} \right] \frac{2(\mu^2 s_1 + \mu_5^2 s_2)}{(\mu^2 + \mu_5^2)} - \frac{1}{2}i\omega, \qquad \tilde{\sigma} = \sigma|_{\mu \leftrightarrow \mu_5},$$

$$\sigma_5 = \tilde{\sigma}_5 = -\left[\underline{\pi\delta(\omega)} + \frac{i}{\omega} \right] \frac{2\mu\mu_5(s_1 - s_2)}{(\mu^2 + \mu_5^2)}. \qquad (4.14)$$

The thermoelectric conductivities are

$$\alpha T = \bar{\alpha}T = \left[\underline{\pi\delta(\omega)} + \frac{i}{\omega} \right] \rho - (\mu\sigma + \mu_5\tilde{\sigma}_5),$$

$$\alpha_5 T = \bar{\alpha}_5 T = \left[\underline{\pi\delta(\omega)} + \frac{i}{\omega} \right] \rho_5 - (\mu\sigma_5 + \mu_5\tilde{\sigma}). \qquad (4.15)$$

Finally, the thermal conductivity is

$$\bar{\kappa}T = \left[\underline{\pi\delta(\omega)} + \frac{i}{\omega} \right] (\mathcal{E} + \mathcal{P} - 2\rho\mu - 2\rho_5\mu_5) + \left(\mu^2\sigma + \mu_5^2\tilde{\sigma} + 2\mu\mu_5\sigma_5 \right). \qquad (4.16)$$

As seen from (4.14)(4.15)(4.16), only σ and σ_5 are independent: $\tilde{\sigma}$ could be extracted from σ via the exchange $\mu \leftrightarrow \mu_5$; all remaining conductivities are determined by their combinations. σ and $\tilde{\sigma}$ are the Ohmic electrical conductivities for vector current and axial current, and σ_5 corresponds to the chiral electric separation effect while $\tilde{\sigma}_5$ is its vector analogue. The CESE conductivity σ_5 is invariant under the exchange of μ and μ_5.

In (4.15), α and α_5 are the thermoelectric conductivities of generating vector and axial currents, respectively. Thanks to time reversal symmetry, Onsager reciprocal relations $\bar{\alpha} = \alpha$ and $\bar{\alpha}_5 = \alpha_5$ do hold, and the conductivity matrix in (4.13) is symmetric. In (4.16), $\bar{\kappa}$ is the heat conductivity. In the numerator of $\bar{\kappa}$, we have made the replacement $\mathcal{E} \to \mathcal{E} + \mathcal{P} = 4M$ as done in [81–83]. This added $\mathcal{P}$ is actually a "contact term" [84] due to translation invariance. Then, it is consistent with (1.21) obtained by fluid/gravity calculations.

Note the appearance of i/ω in the conductivities (4.14)(4.15)(4.16). From the Kramers-Kronig relation [63, 64], this means there must be a delta function $\delta(\omega)$ in real parts of all the conductivities. However, in holographic models with spatial translational invariance, it is not easy to track the delta-peak directly. For consistency, we just added this $\delta(\omega)$ as underlined terms above [63, 64].

In the low-frequency limit where $\omega/T \ll 1$, we obtained analytical expressions for σ, σ_5, see (B.29)(B.30). For the purpose of comparing with (1.17)(1.18), we eliminate bulk parameters in (B.29)(B.30) in favor of thermodynamic quantities of the boundary theory. Eventually, (B.29)(B.30) turn into

$$\sigma = \left[\underline{\pi\delta(\omega)} + \frac{i}{\omega}\right] \frac{\rho^2}{\mathcal{E} + \mathcal{P}} + \sigma_e + \cdots, \quad \sigma_5 = \left[\underline{\pi\delta(\omega)} + \frac{i}{\omega}\right] \frac{\rho_5^2}{\mathcal{E} + \mathcal{P}} + \sigma_{5e} + \cdots, \quad (4.17)$$

where $\cdots$ denote higher powers in ω corrections, σ_e and σ_{5e} are given in (1.8). Obviously, aside from the subtle piece $\delta(\omega)$, the AC conductivities (4.17) are in perfect agreement with the result from linear response (1.17)(1.18). In the single charge limit, (4.17) also stands in line with the two-point correlators of [85]. And in the low-frequency limit, the real part of them give the intrinsic conductivities $\lim_{\omega \to 0} \mathrm{Re}[\sigma] = \sigma_e$ and $\lim_{\omega \to 0} \mathrm{Re}[\sigma_5] = \sigma_{5e}$. The ω-dependence of σ and σ_5 will be the focus of the next subsection.

4.2 AC conductivities: numerical plots

In this subsection, we present numerical results for the AC conductivities σ and σ_5 while depositing more technical details in appendix B. Our results for frequency dependence of Ohmic conductivity σ are plotted in figures 3, 4, 5.

Figure 3 is about the plot of $\sigma/(\pi T)$ as a function of dimensionless frequency $\bar{\omega}$ when either $\bar{\mu} = 0$ or $\bar{\mu}_5 = 0$. As seen from left panels of figure 3, when $\bar{\mu} = 0$, i.e., neglecting the back-reaction effect from the vector field in the bulk, the low-frequency limit of σ is always finite, which is in consistent with the analytical result (4.17). For representative values of $\bar{\mu}_5$ chosen by us, increasing the axial chemical potential $\bar{\mu}_5$ results in reasonably profound modification for the infrared behaviors of σ. From the right-bottom panel of figure 3, it is clear that, once $\bar{\mu} \neq 0$ (i.e. beyond probe limit), there appears divergent behavior for imaginary part of σ: $\mathrm{Im}[\sigma] \sim \bar{\omega}^{-1}$, which is also in agreement with analytical
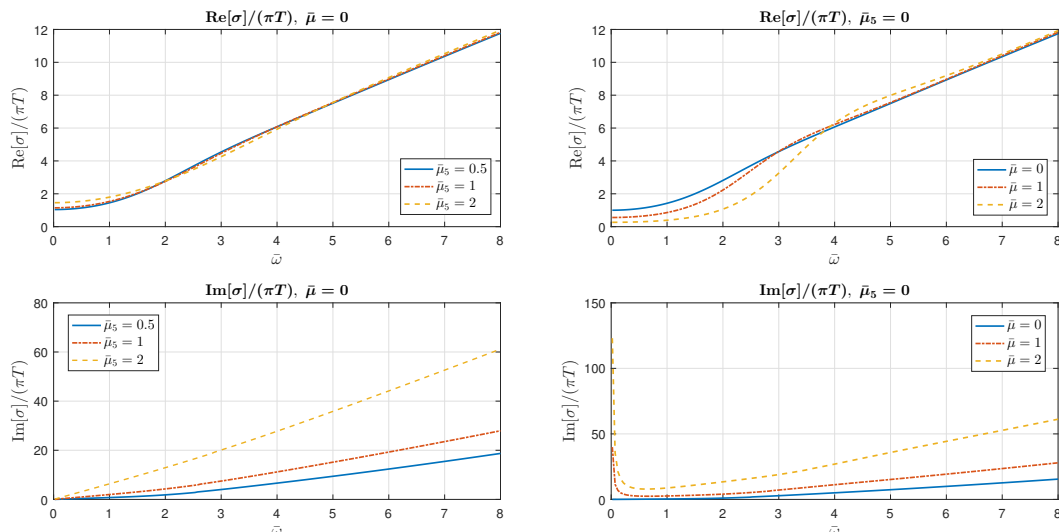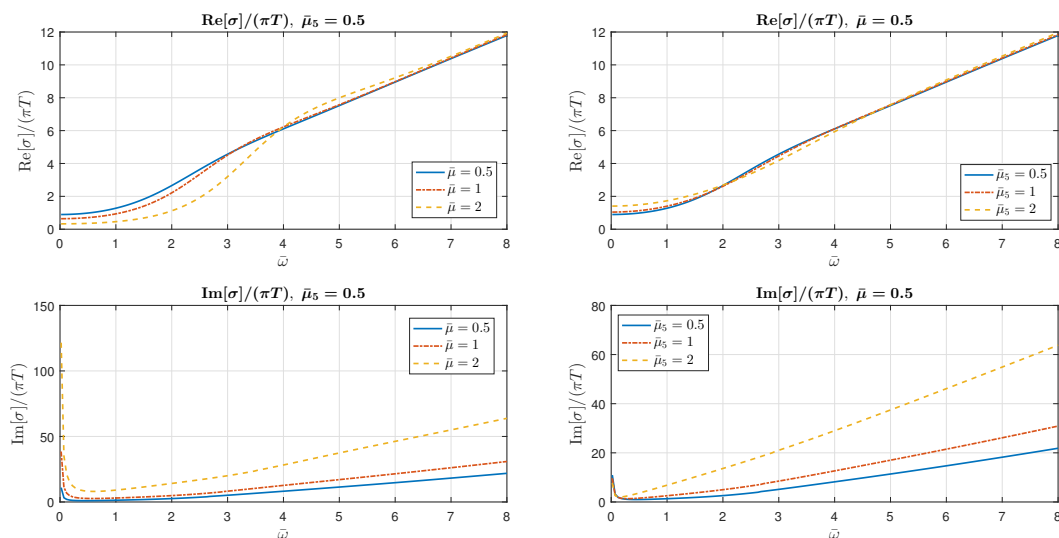
Figure 3. Ohmic conductivity $\sigma/(\pi T)$ (Real and Imaginary parts) as a function of dimensionless frequency $\bar{\omega} = \omega/(\pi T)$ when either $\bar{\mu} = 0$ (left) or $\bar{\mu}_5 = 0$ (right). Different curves correspond to different values of $\bar{\mu}_5 = 0.5, 1, 2$ (left) or $\bar{\mu} = 0, 1, 2$ (right). From the right-bottom panel, there appears divergent behavior for imaginary part of σ: $\text{Im}[\sigma] \sim 1/\bar{\omega}$. Via Kramers-Kronig relation, this implies there should be a delta peak in $\text{Re}[\sigma]$ at $\bar{\omega} = 0$, which we, however, could not track in numerical calculations.

Figure 4. Ohmic conductivity $\sigma/(\pi T)$ (Real and Imaginary parts) as a function of dimensionless frequency $\bar{\omega} = \omega/(\pi T)$ with fixed $\bar{\mu}_5 = 0.5$ (left) or $\bar{\mu} = 0.5$ (right). Different curves correspond to different choices of $\bar{\mu} = 0.5, 1, 2$ (left) or $\bar{\mu}_5 = 0.5, 1, 2$ (right). As in figure 3, the divergent behavior ($\sim 1/\bar{\omega}$) in $\text{Im}[\sigma]$ implies the presence of a delta-peak at $\bar{\omega} = 0$ in $\text{Re}[\sigma]$, which we could not display numerically.

result in (4.17). Via Kramers-Kronig relation, this $1/\bar{\omega}$-behavior in $\text{Im}[\sigma]$ means that $\text{Re}[\sigma] \sim \delta(\bar{\omega})$. Moreover, the strength of back-reaction due to vector field in the bulk is also reflected by different curves in the right-bottom panel in figure 3.
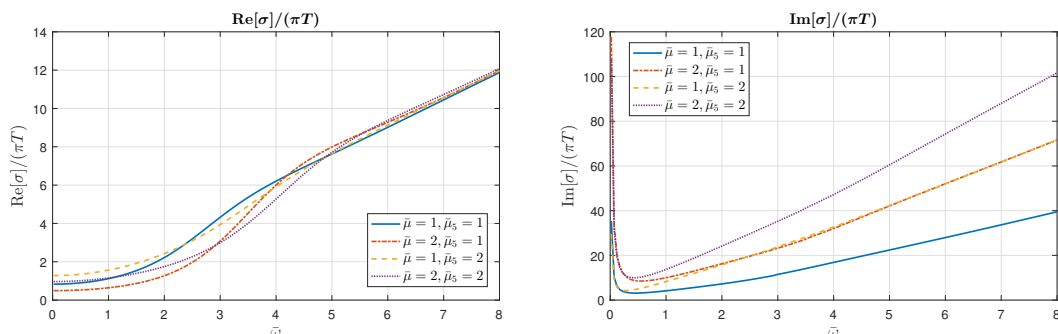
Figure 5. Ohmic conductivity $\sigma/(\pi T)$ (Real and Imaginary parts) as a function of dimensionless frequency $\bar{\omega} = \omega/(\pi T)$ for larger values of $\bar{\mu} = 1, 2$ and $\bar{\mu}_5 = 1, 2$. As in figure 3, the divergent behavior ($\sim 1/\bar{\omega}$) in Im$[\sigma]$ implies the presence of a delta-peak at $\bar{\omega} = 0$ in Re$[\sigma]$, which we could not display numerically.

Figure 4 is to further explore the effects of chemical potentials on σ. In the infrared regime of ω, Im$[\sigma]$ is dominated by the divergent behavior $\sim 1/\bar{\omega}$, which implies a delta-peak $\delta(\omega)$ for Re$[\sigma]$. While we could not display this $\delta(\omega)$ in numerical plots, we find the finite piece in Re$[\sigma]$ and particularly that $\lim_{\omega \to 0}$ Re$[\sigma] = \sigma_e$. Let us focus on the infrared regime (roughly with $0 < \bar{\omega} \lesssim 2$) of Re$[\sigma]$. Our observation is that increasing $\bar{\mu}$ will diminish Re$[\sigma]$ while increasing $\bar{\mu}_5$ will result in enhancement of Re$[\sigma]$. This is exactly consistent with the DC limit σ_e in (1.11), which has been plotted in the left panel of figure 1. The behavior for larger $\bar{\omega}$ is supposed to be controlled by UV conformal symmetry. To confirm this observation, in figure 5 we plot Ohmic conductivity σ, as a function of $\bar{\omega}$, for larger chemical potentials $\bar{\mu}$ and $\bar{\mu}_5$. Roughly, when $\bar{\omega} \gtrsim 6$, Re$[\sigma]$ becomes insensitive to change of chemical potentials.

Figure 6 is to show the frequency-dependence of the CESE conductivity σ_5 and the generalized deviation factor $\chi_A \equiv \sigma_5/(\bar{\mu}\bar{\mu}_5\pi T)$ extending (1.11) to AC case. Given that σ_5 is symmetric under the exchange of μ and μ_5, it is legitimate to constrain to either $\mu \geq \mu_5$ or $\mu \leq \mu_5$ without loss of generality. Just like σ displayed in figures 3, 4, 5, Im$[\sigma_5]$ shows diverging behavior (i.e.$\sim 1/\omega$) near $\omega = 0$, which, via Kramers-Kronig relation, indicates Re$[\sigma] \sim \delta(\omega)$. Once away from $\omega = 0$, the imaginary parts approach zero soon, while the real parts evolve in a more profound fashion as ω is increased. Particularly, we observe a damped oscillating behavior for Re$[\sigma_5]$, where the asymptotic regime is achieved around $\bar{\omega} = 5.5$ for $\mu = 0$. This is roughly in agreement with the numerical results of [31], although we have the different mechanism of generating CESE. Moreover, from figure 6 we observe that increasing μ or $\bar{\mu}_5$ would delay the achievement of the asymptotic regime.

5 Conclusion and discussions

In this work, we explored transport properties of strongly coupled matter, which is holographically described by $(4 + 1)$-dimensional Einstein gravity, coupled to $U(1)_V \times U(1)_A$ gauge fields, in the asymptotic AdS$_5$ black brane. Our main finding is the nonzero CESE conductivity when the gravitational back-reaction effect is taken into account, see (1.11) for
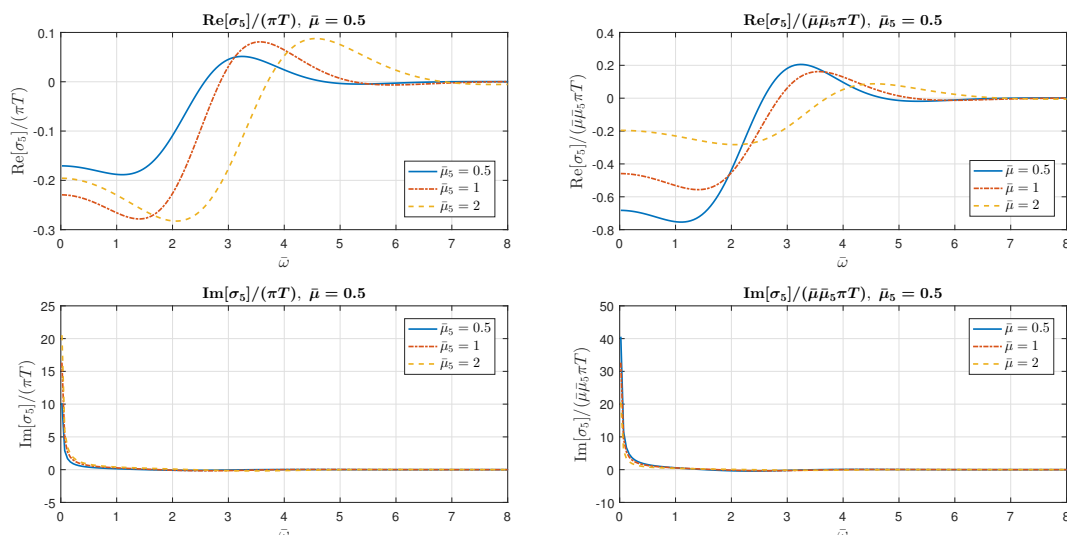
Figure 6. Left: CESE conductivity $\sigma_5/(\pi T)$ (Real and Imaginary parts) as a function of dimensionless frequency $\bar{\omega} = \omega/(\pi T)$. Right: the deviation factor $\sigma_5/(\bar{\mu}\bar{\mu}_5\pi T)$ (Real and Imaginary parts) as a function of $\bar{\omega}$. As in figure 3, the divergent behavior ($\sim 1/\bar{\omega}$) in $\text{Im}[\sigma_5]$ implies the presence of a delta-peak at $\bar{\omega} = 0$ in $\text{Re}[\sigma_5]$, which we could not display numerically.

the hydrodynamic limit and (4.14) for its extension to an AC conductivity. We confirmed our results with two complementary studies — fluid/gravity calculations versus linear response analysis. Within the former framework, we constructed the first-order constitutive relations for stress-energy tensor, vector and axial currents for the holographic matter in the long wavelength and low frequency limit. Following the linear response approach, we revealed the frequency-dependence of Ohmic, CESE and thermoelectric conductivities.

As the second task, we clarified the relations between the dissipative transport coefficients in the hydrodynamic constitutive relations (1.3)(1.4) and those appearing in the conductivity matrix (4.13). While the "intrinsic" conductivities σ_e, σ_{5e} etc. are widely used in the framework of fluid dynamics, the physical observable are indeed those appearing in the conductivity matrix (4.13). Indeed, when the hydrodynamic description is reformulated into the linear response form, we find perfect agreement between these two different approaches, see (1.17)(1.18)(1.20) and (4.17).

Since we have turned off the possible Chern-Simons terms in our holographic model (2.1), it would be interesting to check if the CESE conductivity will be corrected by the chiral anomaly. From recent works [45, 46, 86], the anomalous corrections to normal transport coefficients start from the second order in the derivative expansion. A study along the line of [45, 46, 86] will be helpful in clarifying this issue.

A Technical details in the fluid/gravity calculations

In this appendix, we collect some computational details and useful relations in the fluid/gravity calculations of section 3.

A.1 Solving the bulk equations

Following the standard procedure of fluid/gravity correspondence, we first solve constraint equations to derive relations among fluid-dynamical variables. Practically, we find it more convenient to consider certain combinations of constraint and dynamical equations. Below is the listing of solutions to constraint equations,

$$W^r = 0 \;\Rightarrow\; \partial_t Q + Q_0(\partial_k u_k) = 0, \tag{A.1}$$

$$\tilde{W}^r = 0 \;\Rightarrow\; \partial_t \tilde{Q} + \tilde{Q}_0(\partial_k u_k) = 0, \tag{A.2}$$

$$g^{rr}W_{rt} + g^{rt}W_{tt} = 0 \;\Rightarrow\; 3\partial_t M + 4M_0(\partial_k u_k) = 0, \tag{A.3}$$

$$g^{rr}W_{ri} + g^{rt}W_{ti} = 0 \;\Rightarrow\; \partial_i M + 4M_0 \partial_t u_i = 2\sqrt{3}Q_0 F_{it}^{(\epsilon)}, \tag{A.4}$$

which are, indeed, the hydrodynamic equations (2.15), expanded to the first-order in the derivative expansion. In obtaining (A.4), the first two equations (A.1)(A.2) have been utilized. To proceed, we turn to dynamical equations and find the corrections in (3.7). Dynamical equations will be grouped into the scalar, vector and tensor sectors according to SO(3) symmetry of the boundary spatial directions.

I. Scalar sector. In the scalar sector, we begin with the dynamical equation $E_{rr} = 0$:

$$0 = r\partial_r^2 h(r) + 5\partial_r h(r), \tag{A.5}$$

which is solved by

$$h(r) = C_1^h + \frac{C_2^h}{r^4}. \tag{A.6}$$

The asymptotic condition (3.10) requires $C_1^h = 0$. By Landau-Lifshitz frame condition (3.14), the integration constant C_2^h will also be fixed to zero. Therefore, $h(r) = 0$. From the time components of Maxwell equations $W^t = 0$ and $\tilde{W}^t = 0$,

$$r^3 \partial_r^2 a_t(r) + 3r^2 \partial_r a_t(r) - 4\sqrt{3}Q_0 \partial_r h(r) = 0, \tag{A.7}$$

$$r^3 \partial_r^2 \tilde{a}_t(r) + 3r^2 \partial_r \tilde{a}_t(r) - 4\sqrt{3}\tilde{Q}_0 \partial_r h(r) = 0, \tag{A.8}$$

which are solved by

$$a_t(r) = C_1^a + \frac{C_2^a}{r^2} - \frac{2\sqrt{3}Q_0 C_2^h}{3r^6}, \qquad \tilde{a}_t(r) = C_1^{\tilde{a}} + \frac{C_2^{\tilde{a}}}{r^2} - \frac{2\sqrt{3}\tilde{Q}_0 C_2^h}{3r^6}. \tag{A.9}$$

where $C_1^a, C_2^a, C_1^{\tilde{a}}, C_2^{\tilde{a}}$ are integration constants to be determined by boundary conditions (3.10)–(3.12). First, nonzero $C_1^a, C_1^{\tilde{a}}$ correspond to non-normalizable modes and would violate the asymptotic requirement (3.10). So, $C_1^a = C_1^{\tilde{a}} = 0$. The Landau-Lifshitz frame conditions (3.15) require $C_2^a, C_2^{\tilde{a}}$ to vanish, i.e. $C_2^a = C_2^{\tilde{a}} = 0$. The remaining equation of the scalar sector is $g^{rr}E_{rr} + g^{rt}E_{tr} = 0$,

$$3\partial_r k(r) = (2M_0 - 6r^4)\partial_r h(r) - 24r^3 h(r) + 2\sqrt{3}\left[Q_0 \partial_r a_t(r) + \tilde{Q}_0 \partial_r \tilde{a}_t(r)\right] + 6r^2(\partial_k u_k), \tag{A.10}$$

which is solved by

$$k(r) = \frac{2}{3}r^3(\partial_k u_k) + C_1^k + \frac{2\sqrt{3}(Q_0 C_2^a + \tilde{Q}_0 C_2^{\tilde{a}})}{3r^2} + \left[\frac{2M_0}{3r^4} - \frac{4(Q_0^2 + \tilde{Q}_0^2)}{3r^6}\right]C_2^h. \tag{A.11}$$

A nonzero C_1^k would cause the T_{tt} computed from (3.16) to be in contradiction with the Landau-Lifshitz frame convention (3.14). So, $C_1^k = 0$. Therefore, all the integration constants in the scalar sector have to be set to zero. The solutions in the scalar sector are summarized as below

$$k(r) = \frac{2}{3} r^3 (\partial_k u_k), \qquad h(r) = 0, \qquad a_t(r) = 0, \qquad \tilde{a}_t(r) = 0. \qquad \text{(A.12)}$$

II. Vector sector. Now we consider the helicity one sector, which consists of $a_i(r)$, $\tilde{a}_i(r)$, $j_i(r)$ and turns out to be more involved. First consider the Maxwell equations $W^i = 0$ and $\tilde{W}^i = 0$

$$0 = \partial_r \left[r^3 f_0(r) \partial_r a_i(r) \right] + 2\sqrt{3} Q_0 \partial_r \left(\frac{j_i(r)}{r^4} \right) - \frac{\sqrt{3}}{r^2} (\partial_i Q + Q_0 \partial_t u_i) + F_{ti}^{(\epsilon)}, \qquad \text{(A.13)}$$

$$0 = \partial_r \left[r^3 f_0(r) \partial_r \tilde{a}_i(r) \right] + 2\sqrt{3} \tilde{Q}_0 \partial_r \left(\frac{j_i(r)}{r^4} \right) - \frac{\sqrt{3}}{r^2} \left(\partial_i \tilde{Q} + \tilde{Q}_0 \partial_t u_i \right), \qquad \text{(A.14)}$$

which are dynamical equations for $a_i(r)$ and $\tilde{a}_i(r)$, but coupled to $j_i(r)$. The Einstein equation $W_{ri} = 0$ corresponds to dynamical equation for $j_i(r)$,

$$0 = r \partial_r^2 j_i(r) - 3 \partial_r j_i(r) + 2\sqrt{3} \left[Q_0 \partial_r a_i(r) + \tilde{Q}_0 \partial_r \tilde{a}_i(r) \right] + 3r^2 \partial_t u_i, \qquad \text{(A.15)}$$

which couples to $a_i(r)$ and $\tilde{a}_i(r)$.

Our strategy of solving the coupled differential equations (A.13)–(A.15) is to get rid of $j_i(r)$ and derive decoupled differential equations for suitably combined variables from $a_i(r), \tilde{a}_i(r)$. To this end, we first integrate over r once in the equation (A.15). As a result,

$$0 = r \partial_r j_i(r) - 4 j_i(r) + 2\sqrt{3} \left[Q_0 a_i(r) + \tilde{Q}_0 \tilde{a}_i(r) \right] + r^3 \partial_t u_i, \qquad \text{(A.16)}$$

where the integration constant is fixed by the Landau-Lifshitz frame convention, i.e., in the near boundary expansion for $j_i(r)$ the constant should be zero in order to be consistent with (3.14).

The combinations $Q_0 \times (A.13) + \tilde{Q}_0 \times (A.14)$, and $\tilde{Q}_0 \times (A.13) - Q_0 \times (A.14)$ give rise to

$$0 = \partial_r \left[r^3 f_0(r) \partial_r \left(Q_0 a_i(r) + \tilde{Q}_0 \tilde{a}_i(r) \right) \right] + 2\sqrt{3} (Q_0^2 + \tilde{Q}_0^2) \partial_r \left(\frac{j_i(r)}{r^4} \right)$$
$$- \frac{\sqrt{3}}{r^2} \left[Q_0 \partial_i Q + \tilde{Q}_0 \partial_i \tilde{Q} + (Q_0^2 + \tilde{Q}_0^2) \partial_t u_i \right] + Q_0 F_{ti}^{(\epsilon)}, \qquad \text{(A.17)}$$

and

$$0 = \partial_r \left[r^3 f_0(r) \partial_r \left(\tilde{Q}_0 a_i(r) - Q_0 \tilde{a}_i(r) \right) \right] - \frac{\sqrt{3}}{r^2} (\tilde{Q}_0 \partial_i Q - Q_0 \partial_i \tilde{Q}) + \tilde{Q}_0 F_{ti}^{(\epsilon)}. \qquad \text{(A.18)}$$

Then, substituting (A.16) into (A.17) yields

$$0 = \partial_r \left[r^3 f_0(r) \partial_r \left(Q_0 a_i(r) + \tilde{Q}_0 \tilde{a}_i(r) \right) \right] - \frac{12}{r^5} (Q_0^2 + \tilde{Q}_0^2) \left(Q_0 a_i(r) + \tilde{Q}_0 \tilde{a}_i(r) \right)$$
$$- \frac{\sqrt{3}}{r^2} \left[3(Q_0^2 + \tilde{Q}_0^2) \partial_t u_i + Q_0 \partial_i Q + \tilde{Q}_0 \partial_i \tilde{Q} \right] + Q_0 F_{ti}^{(\epsilon)}. \qquad \text{(A.19)}$$

– 25 –

The equation (A.18) can be solved via direct integration over r,

$$\tilde{Q}_0 a_i(r) - Q_0 \tilde{a}_i(r) = -\int_r^\infty \frac{\mathrm{d}\hat{x}}{\hat{x}^3 f_0(\hat{x})} \int_{r_h}^{\hat{x}} \mathrm{d}y \left[\frac{\sqrt{3}}{y^2} (\tilde{Q}_0 \partial_i Q - Q_0 \partial_i \tilde{Q}_0) - \tilde{Q}_0 F_{ti}^{(\epsilon)} \right]$$

$$\xrightarrow{r\to\infty} \frac{1}{r} \tilde{Q}_0 F_{ti}^{(\epsilon)} - \frac{1}{r^2} \frac{\sqrt{3}}{2r_h} (\tilde{Q}_0 \partial_i Q - Q_0 \partial_i \tilde{Q}) - \frac{1}{r^2} \frac{1}{2} r_h \tilde{Q}_0 F_{ti}^{(\epsilon)} + O\left(r^{-3}\right), \quad \text{(A.20)}$$

where the lower limit of the inner integral is fixed by regularity (3.11) at the unperturbed horizon $r = r_h$ and the upper limit of the outer integral is fixed by asymptotic requirement (3.10).

However, the equation (A.19) is more complicated and cannot be solved by directly integrating over r. Indeed, the homogeneous version of (A.19) has two linearly independent solutions given by $H_1(r) = r^5 f_0'(r)$ and $H_2(r) = H_1(r) \int_r^\infty \mathrm{d}\hat{r} \left[\hat{r}^3 f_0(\hat{r}) H_1(\hat{r})^2 \right]^{-1}$, where the second one $H_2(r)$ is obtained by the Liouville formula. Then, one could proceed to solve (A.19) by using the method of variation of parameters. In practical calculations, we make a coordinate transformation by $u = r_h/r$ and perform the solving of (A.19) in Mathematica. The regularity at the unperturbed horizon and asymptotic requirement completely fix both integration constants. Since the final solution looks quite complicated, we only record the large r behavior for $Q_0 a_i(r) + \tilde{Q}_0 \tilde{a}_i(r)$,

$$Q_0 a_i(r) + \tilde{Q}_0 \tilde{a}_i(r) \xrightarrow{r\to\infty} -\frac{1}{r^2} \frac{\sqrt{3}(2r_h^6 + Q_0^2 + \tilde{Q}_0^2)}{4M_0 r_h^3} \left[3(Q_0^2 + \tilde{Q}_0^2) \partial_t u_i + Q_0 \partial_i Q + \tilde{Q}_0 \partial_i \tilde{Q} \right]$$

$$+ \frac{1}{r} Q_0 F_{ti}^{(\epsilon)} - \frac{1}{r^2} \left[\frac{3(Q_0^2 + \tilde{Q}_0^2)}{4M_0 r_h} + \frac{1}{2} r_h \right] Q_0 F_{ti}^{(\epsilon)} + O\left(r^{-3}\right). \quad \text{(A.21)}$$

Therefore, the near boundary behaviors for $a_i(r)$ and $\tilde{a}_i(r)$ are

$$a_i(r) \xrightarrow{r\to\infty} -\frac{3\sqrt{3}Q_0}{r^2} \left(\frac{r_h^3}{4M_0} + \frac{1}{4r_h} \right) \partial_t u_i - \frac{\sqrt{3}}{r^2} \frac{(2r_h^6 + Q_0^2 + 2\tilde{Q}_0^2)}{4M_0 r_h^3} \partial_i Q + \frac{\sqrt{3}}{r^2} \frac{Q_0 \tilde{Q}_0}{4M_0 r_h^3} \partial_i \tilde{Q}$$

$$+ \frac{1}{r} F_{ti}^{(\epsilon)} - \frac{1}{r^2} \left(\frac{3Q_0^2}{4M_0 r_h} + \frac{1}{2} r_h \right) F_{ti}^{(\epsilon)} + O\left(r^{-3}\right), \quad \text{(A.22)}$$

$$\tilde{a}_i(r) \xrightarrow{r\to\infty} -\frac{3\sqrt{3}\tilde{Q}_0}{r^2} \left(\frac{r_h^3}{4M_0} + \frac{1}{4r_h} \right) \partial_t u_i - \frac{\sqrt{3}}{r^2} \frac{(2r_h^6 + 2Q_0^2 + \tilde{Q}_0^2)}{4M_0 r_h^3} \partial_i \tilde{Q} + \frac{\sqrt{3}}{r^2} \frac{Q_0 \tilde{Q}_0}{4M_0 r_h^3} \partial_i Q$$

$$- \frac{1}{r^2} \frac{3Q_0 \tilde{Q}_0}{4M_0 r_h} F_{ti}^{(\epsilon)} + O\left(r^{-3}\right). \quad \text{(A.23)}$$

With large r behaviors of $a_i(r), \tilde{a}_i(r)$ at hand, the equation (A.16) could be solved near the boundary $r = \infty$, yielding

$$j_i(r) \xrightarrow{r\to\infty} r^3 \partial_t u_i + O(r^{-1}). \quad \text{(A.24)}$$

III. Tensor sector. Finally, the tensor equation $W_{ij} - \frac{1}{3} \delta_{ij} W_{kk} = 0$ gives the dynamical equation for $\alpha_{ij}(r)$:

$$\partial_r \left[r^5 f_0(r) \partial_r \alpha_{ij}(r) \right] + 3r^2 \left[\partial_i u_j + \partial_j u_i - \frac{2}{3} \delta_{ij} (\partial_k u_k) \right] = 0, \quad \text{(A.25)}$$

which can be solved by direct integration over r. The final solution for $\alpha_{ij}(r)$ is

$$\alpha_{ij}(r) = 3\left[\partial_i u_j + \partial_j u_i - \frac{2}{3}\delta_{ij}(\partial_k u_k)\right]\int_\infty^r \frac{\mathrm{d}\hat{x}}{\hat{x}^5 f_0(\hat{x})}\int_{r_h}^{\hat{x}} y^2 \mathrm{d}y,$$

$$\xrightarrow{r\to\infty} \left(\frac{1}{r} - \frac{r_h^3}{4r^4}\right)\left[\partial_i u_j + \partial_j u_i - \frac{2}{3}\delta_{ij}(\partial_k u_k)\right] + O(r^{-5}). \tag{A.26}$$

A.2 Useful relations in deriving dual currents

In this appendix, we summarize some formulas that are quite lengthy but useful towards deriving non-anomalous parts of the currents in (1.3)(1.4). From (3.19)(3.20), armed with the near-boundary behaviors derived in appendix A.1, the vector and axial currents of the boundary theory are

$$J^t = 2\sqrt{3}Q, \qquad\qquad J_5^t = 2\sqrt{3}\tilde{Q}, \tag{A.27}$$

$$J^i = \sqrt{3}Q_0 u_i - 3\sqrt{3}Q_0\left(\frac{r_h^3}{2M_0} + \frac{1}{2r_h}\right)\partial_t u_i - \frac{\sqrt{3}(2r_h^6 + Q_0^2 + 2\tilde{Q}_0^2)}{2M_0 r_h^3}\partial_i Q$$

$$+ \frac{\sqrt{3}Q_0\tilde{Q}_0}{2M_0 r_h^3}\partial_i\tilde{Q} - \left(\frac{3Q_0^2}{2M_0 r_h} + r_h\right)F_{ti}^{(\epsilon)}, \tag{A.28}$$

$$J_5^i = \sqrt{3}\tilde{Q}_0 u_i - 3\sqrt{3}\tilde{Q}_0\left(\frac{r_h^3}{2M_0} + \frac{1}{2r_h}\right)\partial_t u_i - \frac{\sqrt{3}(2r_h^6 + 2Q_0^2 + \tilde{Q}_0^2)}{2M_0 r_h^3}\partial_i\tilde{Q}$$

$$+ \frac{\sqrt{3}Q_0\tilde{Q}_0}{2M_0 r_h^3}\partial_i Q - \frac{3Q_0\tilde{Q}_0}{2M_0 r_h}F_{ti}^{(\epsilon)}, \tag{A.29}$$

where $\partial_t u_i$ will be replaced via the constraint relation (A.4)

$$\partial_t u_i = -\frac{\partial_i M}{4M_0} - \frac{\sqrt{3}Q_0}{2M_0}F_{ti}^{(\epsilon)}. \tag{A.30}$$

Meanwhile, the derivative $\partial_i M$ would be replaced by

$$\partial_i M = \frac{1}{r_h^3}\left(Q_0\partial_i Q + \tilde{Q}_0\partial_i\tilde{Q}\right) + 2r_h^3\left(1 - \frac{Q_0^2 + \tilde{Q}_0^2}{2r_h^6}\right)\partial_i r_h, \tag{A.31}$$

which is obtained by expanding

$$1 - \frac{M}{r_h^4} + \frac{Q^2 + \tilde{Q}^2}{r_h^6} = 0, \tag{A.32}$$

around $x^\mu = 0$ up to first-order in derivative expansion.

Then, the derivative terms in (A.28)(A.29) are linear combinations of $\partial_i r_h$, $\partial_i Q$ and $\partial_i\tilde{Q}$, which have to be re-parameterized in terms of derivatives of fluid-dynamical variables. Via the relations (3.31)(3.32), it is straightforward although tedious to derive the following expressions

$$\frac{\partial_i T}{T} = -\frac{2\left(Q_0\partial_i Q + \tilde{Q}_0\partial_i\tilde{Q}\right)}{2r_h^6 - Q_0^2 - \tilde{Q}_0^2} + \frac{2r_h^6 + 5\left(Q_0^2 + \tilde{Q}_0^2\right)}{\left(2r_h^6 - Q_0^2 - \tilde{Q}_0^2\right)}\frac{\partial_i r_h}{r_h}, \tag{A.33}$$

$$\partial_i\left(\frac{\mu}{T}\right) = \frac{2\sqrt{3}\pi r_h^2\left(r_h\partial_i Q - 3Q_0\partial_i r_h\right)}{2r_h^6 - Q_0^2 - \tilde{Q}_0^2} + \frac{4\sqrt{3}\pi Q_0 r_h^2\left(r_h Q_0\partial_i Q + r_h\tilde{Q}_0\partial_i\tilde{Q} - 3Q_0^2\partial_i r_h - 3\tilde{Q}_0^2\partial_i r_h\right)}{\left(2r_h^6 - Q_0^2 - \tilde{Q}_0^2\right)^2}, \tag{A.34}$$

$$\partial_i\left(\frac{\mu_5}{T}\right) = \frac{2\sqrt{3}\pi r_h^2\left(r_h\partial_i\tilde{Q} - 3\tilde{Q}_0\partial_i r_h\right)}{2r_h^6 - Q_0^2 - \tilde{Q}_0^2} + \frac{4\sqrt{3}\pi\tilde{Q}_0 r_h^2\left(r_h Q_0\partial_i Q + r_h\tilde{Q}_0\partial_i\tilde{Q} - 3Q_0^2\partial_i r_h - 3\tilde{Q}_0^2\partial_i r_h\right)}{\left(2r_h^6 - Q_0^2 - \tilde{Q}_0^2\right)^2}, \tag{A.35}$$

which could be inverted to express $\partial_i r_h$, $\partial_i Q$ and $\partial_i\tilde{Q}$ in terms of $\partial_i T$, $\partial_i(\mu/T)$ and $\partial_i(\mu_5/T)$.

B Technical details in linear response analysis

In this appendix, we collect calculation details in the linear response analysis presented in section 4.

I. Identify external sources. According to the holographic dictionary, non-normalizable modes of bulk fields act as external sources. Thus, near the conformal boundary $r \to \infty$, we require

$$\delta g_{ti}(r,t) = r^2\big[\delta h_{ti}^{(0)}(t) + O(r^{-1})\big], \tag{B.1}$$

$$\delta A_i(r,t) = \delta a_i^{(0)}(t) + O(r^{-1}), \tag{B.2}$$

$$\delta \tilde{A}_i(r,t) = \delta \tilde{a}_i^{(0)}(t) + O(r^{-1}). \tag{B.3}$$

As a result, the boundary metric is perturbed to be $\eta_{\mu\nu} + \delta h_{ti}^{(0)}(t)$. The purpose of introducing a boundary metric perturbation $\delta h_{ti}^{(0)}(t)$ is to turn on a thermal gradient $\nabla_i T$. Indeed, via the diffeomorphism invariance, one could show that a thermal gradient $\nabla_i T$ leads to a boundary metric perturbation $\delta h_{ti}^{(0)}(t)$ [81, 82],

$$i\omega \delta h_{tj}^{(0)} = -\frac{\nabla_j T}{T}. \tag{B.4}$$

On the other hand, a thermal gradient $\nabla_i T$ also induces perturbations to boundary vector and axial gauge potentials,

$$i\omega \delta a_j^{(\mathrm{T})} = \mu \frac{\nabla_j T}{T}, \qquad i\omega \delta \tilde{a}_j^{(\mathrm{T})} = \mu_5 \frac{\nabla_j T}{T}, \tag{B.5}$$

where the superscript $^{(\mathrm{T})}$ is to emphasize that the potential perturbations in (B.5) are generated by a thermal gradient and will be vanishing once the thermal gradient is turned off. The chemical potentials μ, μ_5 are defined as in (3.31). Consequently, we identify external vector and axial electric fields as

$$\begin{aligned}
E_i &= -\partial_t\big(\delta a_i^{(0)} - \delta a_i^{(\mathrm{T})}\big) = i\omega\big(\delta a_i^{(0)} + \mu \delta h_{ti}^{(0)}\big), \\
E_i^5 &= -\partial_t\big(\delta \tilde{a}_i^{(0)} - \delta \tilde{a}_i^{(\mathrm{T})}\big) = i\omega\big(\delta \tilde{a}_i^{(0)} + \mu_5 \delta h_{ti}^{(0)}\big).
\end{aligned} \tag{B.6}$$

In (B.4)–(B.6) we have assumed plane wave ansatz for external perturbations

$$\delta h_{ti}^{(0)}(t) \sim e^{-i\omega t}\delta h_{ti}^{(0)}(\omega), \qquad \delta a_i^{(0)}(t) \sim e^{-i\omega t}\delta a_i^{(0)}(\omega), \qquad \delta \tilde{a}_i^{(0)}(t) \sim e^{-i\omega t}\delta \tilde{a}_i^{(0)}(\omega). \tag{B.7}$$

II. Bulk equations linearized. To linear order in perturbations, the bulk equations of motion (2.7)–(2.9) become

$$W_{ri} = 0 \;\Rightarrow\; 0 = r^3\partial_r^2\delta g_{ti} + r^2\partial_r\delta g_{ti} - 4r\delta g_{ti} + 2\sqrt{3}\partial_r\big(Q\delta A_i + \tilde{Q}\delta \tilde{A}_i\big), \tag{B.8}$$

$$\begin{aligned}
W_{ti} = 0 \;\Rightarrow\; 0 = {}& r^5 f(r)\partial_r^2\delta g_{ti} + r^4 f(r)\partial_r\delta g_{ti} + r^3\partial_r\partial_t\delta g_{ti} - 2r^2\partial_t\delta g_{ti} \\
& - 4r^3 f(r)\delta g_{ti} + 2\sqrt{3}\big[r^2 f(r)\partial_r + \partial_t\big]\big(Q\delta A_i + \tilde{Q}\delta \tilde{A}_i\big),
\end{aligned} \tag{B.9}$$

as well as

$$
\begin{aligned}
W^i = 0 \;\Rightarrow\; 0 &= r^3 f(r) \partial_r^2 \delta A_i + \partial_r \left[r^3 f(r) \right] \partial_r \delta A_i + 2r \partial_r \partial_t \delta A_i + \partial_t \delta A_i \\
&\quad + 2\sqrt{3} Q r^{-3} \left(r \partial_r \delta g_{ti} - 2\delta g_{ti} \right),
\end{aligned}
\tag{B.10}
$$

$$
\begin{aligned}
\tilde{W}^i = 0 \;\Rightarrow\; 0 &= r^3 f(r) \partial_r^2 \delta \tilde{A}_i + \partial_r \left[r^3 f(r) \right] \partial_r \delta \tilde{A}_i + 2r \partial_r \partial_t \delta \tilde{A}_i + \partial_t \delta \tilde{A}_i \\
&\quad + 2\sqrt{3} \tilde{Q} r^{-3} \left(r \partial_r \delta g_{ti} - 2\delta g_{ti} \right).
\end{aligned}
\tag{B.11}
$$

The combination $r^2 f(r) W_{ri} - W_{ti} = 0$ results in a simpler equation

$$
0 = r^3 \partial_r \delta g_{ti} - 2r^2 \delta g_{ti} + 2\sqrt{3}(\tilde{Q} \delta \tilde{A}_i + Q \delta A_i),
\tag{B.12}
$$

which helps to decouple δA_i, $\delta \tilde{A}_i$ from δg_{ti}. As a result,

$$
0 = \partial_r \left[r^3 f(r) \partial_r \delta A_i \right] + 2r \partial_r \partial_t \delta A_i + \partial_t \delta A_i - 12 Q r^{-5} (Q \delta A_i + \tilde{Q} \delta \tilde{A}_i),
\tag{B.13}
$$

$$
0 = \partial_r \left[r^3 f(r) \partial_r \delta \tilde{A}_i \right] + 2r \partial_r \partial_t \delta \tilde{A}_i + \partial_t \delta \tilde{A}_i - 12 \tilde{Q} r^{-5} (Q \delta A_i + \tilde{Q} \delta \tilde{A}_i).
\tag{B.14}
$$

To proceed, we define the variables

$$
\begin{aligned}
X_i &\equiv Q \delta A_i + \tilde{Q} \delta \tilde{A}_i - (Q \delta a_i^{(0)} + \tilde{Q} \delta \tilde{a}_i^{(0)}), \\
Y_i &\equiv \tilde{Q} \delta A_i - Q \delta \tilde{A}_i - (\tilde{Q} \delta a_i^{(0)} - Q \delta \tilde{a}_i^{(0)}),
\end{aligned}
\tag{B.15}
$$

so that $\lim_{r \to \infty} X_i \to 0$, and $\lim_{r \to \infty} Y_i \to 0$. Then, the equations (B.13)(B.14) turn into decoupled equations for X_i and Y_i,

$$
\begin{aligned}
0 &= \partial_r \left[r^3 f(r) \partial_r X_i \right] + 2r \partial_r \partial_t X_i + \partial_t X_i - 12(Q^2 + \tilde{Q}^2) r^{-5} X_i \\
&\quad + \left[\partial_t - 12(Q^2 + \tilde{Q}^2) r^{-5} \right] (Q \delta a_i^{(0)} + \tilde{Q} \delta \tilde{a}_i^{(0)}),
\end{aligned}
\tag{B.16}
$$

$$
0 = \partial_r \left[r^3 f(r) \partial_r Y_i \right] + 2r \partial_r \partial_t Y_i + \partial_t Y_i + \partial_t \left(\tilde{Q} \delta a_i^{(0)} - Q \delta \tilde{a}_i^{(0)} \right).
\tag{B.17}
$$

Inspired by the structure of source terms in (B.16)(B.17), we could factorize X_i and Y_i as

$$
\begin{aligned}
X_i(r, t) &= S_1(r, \partial_t) \left[Q \delta a_i^{(0)}(t) + \tilde{Q} \delta \tilde{a}_i^{(0)}(t) \right], \\
Y_i(r, t) &= S_2(r, \partial_t) \left[Q \delta a_i^{(0)}(t) + \tilde{Q} \delta \tilde{a}_i^{(0)}(t) \right].
\end{aligned}
\tag{B.18}
$$

In Fourier space by $\partial_t \to -i\omega$, we have $S_1(r, \partial_t) \to S_1(r, \omega)$, $S_2(r, \partial_t) \to S_2(r, \omega)$. Eventually, dynamical equations for $\delta A_i, \delta \tilde{A}_i$ turn into decoupled ordinary differential equations for scalar functions S_1, S_2:

$$
0 = \partial_r \left[r^3 f(r) \partial_r S_1 \right] - 2i\omega r \partial_r S_1 - i\omega S_1 - 12(Q^2 + \tilde{Q}^2) r^{-5} S_1 - i\omega - 12(Q^2 + \tilde{Q}^2) r^{-5},
\tag{B.19}
$$

$$
0 = \partial_r \left[r^3 f(r) \partial_r S_2 \right] - 2i\omega r \partial_r S_2 - i\omega S_2 - i\omega.
\tag{B.20}
$$

The asymptotic expansions of δA_i and $\delta \tilde{A}_i$ in (4.5)(4.6) get translated into near boundary behavior for S_1, S_2, which we sketchily summarise as

$$
S_i \xrightarrow{r \to \infty} \frac{s_i^{(1)}}{r} + \frac{s_i}{r^2} + \frac{\log r}{r^2} s_i^{\mathrm{L}}, \qquad i = 1, 2,
\tag{B.21}
$$

where $s_i^{(1)}, s_i^{\mathrm{L}}$ are easily read off from (4.5)(4.6) and s_i will be solved in the following. Afterwards, we determine the frequency-dependence of conductivities σ and σ_{5e}.

We turn to a bounded radial coordinate by the transformation,

$$u \equiv \frac{r_h}{r} \Rightarrow u \in [0, 1], \tag{B.22}$$

so that the conformal boundary is located at $u = 0$ and the event horizon is at $u = 1$. In the u-coordinate, equations (B.19)(B.20) are turned into

$$0 = u^2 \partial_u \left[u^{-1} f(u) \partial_u S_1 \right] + 2i\hat{\omega} u \partial_u S_1 - i\hat{\omega}(S_1 + 1) - 4\left(\hat{\mu}^2 + \hat{\mu}_5^2\right) u^5 \left(S_1 + 1\right),$$
$$0 = u^2 \partial_u \left[u^{-1} f(u) \partial_u S_2 \right] + 2i\hat{\omega} u \partial_u S_2 - i\hat{\omega}\left(S_2 + 1\right), \tag{B.23}$$

where

$$\hat{\omega} = \frac{\omega}{r_h}, \qquad \hat{\mu} = \frac{\mu}{r_h}, \qquad \hat{\mu}_5 = \frac{\mu_5}{r_h}, \qquad f(u) = 1 - u^4 + \frac{1}{3}\left(\hat{\mu}^2 + \hat{\mu}_5^2\right) u^4(u^2 - 1). \tag{B.24}$$

The equations (B.23) will be first solved analytically in the hydrodynamic limit to compare with the results of section 3 and then numerically in order to reveal the frequency dependence of conductivities.

III. Hydrodynamic limit. First, we consider the hydrodynamic limit where $\hat{\omega} \ll 1$ so that we could compute σ and σ_{5e} analytically. Introduce a formal parameter by the rescaling $\hat{\omega} \to \lambda\hat{\omega}$. Then, S_1, S_2 are expanded as $S_1 = \sum_{n=0}^{\infty} \lambda^n S_1^{[n]}, S_2 = \sum_{n=0}^{\infty} \lambda^n S_2^{[n]}$. To the zeroth order $O(\lambda^0)$,

$$S_1^{[0]} = -\frac{3\left(\hat{\mu}^2 + \hat{\mu}_5^2\right)}{2\left(3 + \hat{\mu}^2 + \hat{\mu}_5^2\right)} u^2, \qquad S_2^{[0]} = 0. \tag{B.25}$$

To the first-order $O(\lambda^1)$, $S_2^{[1]}$ can be solved by direct integration over r and the result is

$$S_2^{[1]} = i\hat{\omega} \int_0^u \frac{\hat{x}\mathrm{d}\hat{x}}{f(\hat{x})} \int_1^{\hat{x}} \frac{\mathrm{d}y}{y^2} \xrightarrow{u \to 0} \frac{1}{2} i\hat{\omega}\left(-2u + u^2\right) + O(u^3). \tag{B.26}$$

The equation for $S_1^{[1]}$ is

$$0 = u^2 \partial_u \left[u^{-1} f(u) \partial_u S_1^{[1]} \right] - 4\left(\hat{\mu}^2 + \hat{\mu}_5^2\right) u^5 S_1^{[1]} + 2i\hat{\omega} u \partial_u S_1^{[0]} - i\hat{\omega} S_1^{[0]} - i\hat{\omega}, \tag{B.27}$$

which we solved by using Mathematica's DSolve command. The integration constants are fixed by regularity at $u = 1$ and asymptotic requirement at the boundary $u = 0$. Given that the final solution for $S_1^{[1]}$ is quite lengthy, we record its near boundary expansion only,

$$S_1^{[1]} \xrightarrow{u \to 0} -i\hat{\omega} u + i\hat{\omega} u^2 \frac{\left(-6 + \hat{\mu}^2 + \hat{\mu}_5^2\right)}{\left(3 + \hat{\mu}^2 + \hat{\mu}_5^2\right)} + O(u^3), \tag{B.28}$$

which is enough for calculating the conductivities.

Recall the AC Conductivities (4.14) and the near boundary behaviors in (B.21), the small ω limits of conductivities σ, σ_5 are

$$\sigma = \frac{i}{\omega} \frac{3Q^2 r_h^2}{r_h^6 + Q^2 + \tilde{Q}^2} + \frac{Q^4 + Q^2(5\tilde{Q}^2 - 4r_h^6) + 4(\tilde{Q}^2 + r_h^6)^2}{4(r_h^6 + Q^2 + \tilde{Q}^2)^2} r_h + \cdots, \quad \text{(B.29)}$$

$$\sigma_5 = \frac{i}{\omega} \frac{3Q\tilde{Q} r_h^2}{r_h^6 + Q^2 + \tilde{Q}^2} - \frac{3Q\tilde{Q}(4r_h^6 + Q^2 + \tilde{Q}^2)}{4(r_h^6 + Q^2 + \tilde{Q}^2)} r_h + \cdots, \quad \text{(B.30)}$$

where $\cdots$ denote higher powers in ω corrections. Results above are in perfect agreement with the linear response limit of fluid/gravity calculations (1.17)(1.18) by utilizing the following relation $M = r_h^4 + (Q^2 + \tilde{Q}^2)/r_h^2$, as well as taking into account (1.8).

IV. Numerical technique. For generic frequency ω, we were able to solve ODEs in (B.23) numerically only. Inspired by the expressions (4.14) we turn to variables

$$S_+ = \frac{\hat{\mu}^2 S_1 + \hat{\mu}_5^2 S_2}{\hat{\mu}^2 + \hat{\mu}_5^2}, \qquad S_- = \frac{\hat{\mu}\hat{\mu}_5 (S_1 - S_2)}{\hat{\mu}^2 + \hat{\mu}_5^2}, \quad \text{(B.31)}$$

which obey coupled ODEs,

$$0 = u^2 \partial_u \left[u^{-1} f(u) \partial_u S_+ \right] + 2i\hat{\omega} u \partial_u S_+ - i\hat{\omega}(S_+ + 1) - 4u^5 \hat{\mu} \left(\hat{\mu} S_+ + \hat{\mu}_5 S_- + \hat{\mu} \right),$$
$$0 = u^2 \partial_u \left[u^{-1} f(u) \partial_u S_- \right] + 2i\hat{\omega} u \partial_u S_- - i\hat{\omega} S_- - 4u^5 \hat{\mu}_5 \left(\hat{\mu} S_+ + \hat{\mu}_5 S_- + \hat{\mu} \right). \quad \text{(B.32)}$$

We numerically solve (B.32) within the pseudospectral collocation method. The boundary conditions for S_+, S_- could be straightforwardly obtained from those for S_1, S_2. For the sake of performing numerical calculations within the spectral collocation method, we summarize the boundary conditions as equalities

$$S_+ = S_- = 0, \qquad \text{at} \qquad u = 0, \quad \text{(B.33)}$$

$$\left\{ \left[-4 + \frac{2}{3}(\hat{\mu}^2 + \hat{\mu}_5^2) + 2i\hat{\omega} \right] \partial_u S_+ - i\hat{\omega}(S_+ + 1) - 4\hat{\mu} \left(\hat{\mu} S_+ + \hat{\mu}_5 S_- + \hat{\mu} \right) \right\} \bigg|_{u=1} = 0, \quad \text{(B.34)}$$

$$\left\{ \left[-4 + \frac{2}{3}(\hat{\mu}^2 + \hat{\mu}_5^2) + 2i\hat{\omega} \right] \partial_u S_- - i\hat{\omega} S_- - 4\hat{\mu}_5 \left(\hat{\mu} S_+ + \hat{\mu}_5 S_- + \hat{\mu} \right) \right\} \bigg|_{u=1} = 0. \quad \text{(B.35)}$$

With equations (B.32) solved, AC conductivities σ, σ_5 are extracted from the near boundary behavior of S_+ and S_-:

$$\sigma = \frac{r_h^2}{i\omega} \partial_u^2 \left(S_+ + \frac{1}{2}\omega^2 u^2 \log u \right) \bigg|_{u=0} - \frac{1}{2} i\omega, \qquad \sigma_5 = \frac{r_h^2}{i\omega} \partial_u^2 S_- \bigg|_{u=0}. \quad \text{(B.36)}$$

Acknowledgments

References

[1] D. Kharzeev, *Parity violation in hot QCD: Why it can happen and how to look for it*, *Phys. Lett.* **B 633** (2006) 260 [`hep-ph/0406125`] [ɪɴSPIRE].

[2] D. Kharzeev and A. Zhitnitsky, *Charge separation induced by P-odd bubbles in QCD matter*, *Nucl. Phys.* **A 797** (2007) 67 [`arXiv:0706.1026`] [ɪɴSPIRE].

[3] D.E. Kharzeev, L.D. McLerran and H.J. Warringa, *The Effects of topological charge change in heavy ion collisions: 'Event by event P and CP-violation'*, *Nucl. Phys.* **A 803** (2008) 227 [`arXiv:0711.0950`] [ɪɴSPIRE].

[4] K. Fukushima, D.E. Kharzeev and H.J. Warringa, *The Chiral Magnetic Effect*, *Phys. Rev.* **D 78** (2008) 074033 [`arXiv:0808.3382`] [ɪɴSPIRE].

[5] J. Erdmenger, M. Haack, M. Kaminski and A. Yarom, *Fluid dynamics of R-charged black holes*, *JHEP* **01** (2009) 055 [`arXiv:0809.2488`] [ɪɴSPIRE].

[6] N. Banerjee, J. Bhattacharya, S. Bhattacharyya, S. Dutta, R. Loganayagam and P. Surowka, *Hydrodynamics from charged black branes*, *JHEP* **01** (2011) 094 [`arXiv:0809.2596`] [ɪɴSPIRE].

[7] D.T. Son and P. Surowka, *Hydrodynamics with Triangle Anomalies*, *Phys. Rev. Lett.* **103** (2009) 191601 [`arXiv:0906.5044`] [ɪɴSPIRE].

[8] D.T. Son and A.R. Zhitnitsky, *Quantum anomalies in dense matter*, *Phys. Rev.* **D 70** (2004) 074018 [`hep-ph/0405216`] [ɪɴSPIRE].

[9] M.A. Metlitski and A.R. Zhitnitsky, *Anomalous axion interactions and topological currents in dense matter*, *Phys. Rev.* **D 72** (2005) 045011 [`hep-ph/0505072`] [ɪɴSPIRE].

[10] D.E. Kharzeev and H.-U. Yee, *Chiral Magnetic Wave*, *Phys. Rev.* **D 83** (2011) 085007 [`arXiv:1012.6026`] [ɪɴSPIRE].

[11] Y. Burnier, D.E. Kharzeev, J. Liao and H.-U. Yee, *Chiral magnetic wave at finite baryon density and the electric quadrupole moment of quark-gluon plasma in heavy ion collisions*, *Phys. Rev. Lett.* **107** (2011) 052303 [`arXiv:1103.1307`] [ɪɴSPIRE].

[12] D.E. Kharzeev and D.T. Son, *Testing the chiral magnetic and chiral vortical effects in heavy ion collisions*, *Phys. Rev. Lett.* **106** (2011) 062301 [`arXiv:1010.0038`] [ɪɴSPIRE].

[13] A. Bzdak, V. Koch and J. Liao, *Charge-Dependent Correlations in Relativistic Heavy Ion Collisions and the Chiral Magnetic Effect*, *Lect. Notes Phys.* **871** (2013) 503 [`arXiv:1207.7327`] [ɪɴSPIRE].

[14] H.-U. Yee and Y. Yin, *Realistic Implementation of Chiral Magnetic Wave in Heavy Ion Collisions*, *Phys. Rev.* **C 89** (2014) 044909 [arXiv:1311.2574] [ɪɴSPIRE].

[15] ALICE collaboration, *Charge-dependent flow and the search for the chiral magnetic wave in Pb-Pb collisions at* $\sqrt{s_{\mathrm{NN}}} = 2.76$ *TeV*, *Phys. Rev.* **C 93** (2016) 044903 [arXiv:1512.05739] [ɪɴSPIRE].

[16] CMS collaboration, *Observation of charge-dependent azimuthal correlations in p-Pb collisions and its implication for the search for the chiral magnetic effect*, *Phys. Rev. Lett.* **118** (2017) 122301 [arXiv:1610.00263] [ɪɴSPIRE].

[17] CMS collaboration, *Constraints on the chiral magnetic effect using charge-dependent azimuthal correlations in pPb and PbPb collisions at the CERN Large Hadron Collider*, *Phys. Rev.* **C 97** (2018) 044912 [arXiv:1708.01602] [ɪɴSPIRE].

[18] CMS collaboration, *Challenges to the chiral magnetic wave using charge-dependent azimuthal anisotropies in pPb and PbPb collisions at* $\sqrt{s_{\mathrm{NN}}} = 5.02$ *TeV*, arXiv:1708.08901 [ɪɴSPIRE].

[19] X. Huang et al., *Observation of the Chiral-Anomaly-Induced Negative Magnetoresistance in 3D Weyl Semimetal TaAs*, *Phys. Rev.* **X 5** (2015) 031023 [arXiv:1503.01304] [ɪɴSPIRE].

[20] H. Li et al., *Negative Magnetoresistance in Dirac Semimetal Cd3As2*, *Nat. Commun.* **7** (2016) 10301 [arXiv:1507.06470].

[21] Q. Li et al., *Observation of the chiral magnetic effect in ZrTe5*, *Nature Phys.* **12** (2016) 550 [arXiv:1412.6543] [ɪɴSPIRE].

[22] D.E. Kharzeev, *The Chiral Magnetic Effect and Anomaly-Induced Transport*, *Prog. Part. Nucl. Phys.* **75** (2014) 133 [arXiv:1312.3348] [ɪɴSPIRE].

[23] X.-G. Huang, *Electromagnetic fields and anomalous transports in heavy-ion collisions — A pedagogical review*, *Rept. Prog. Phys.* **79** (2016) 076302 [arXiv:1509.04073] [ɪɴSPIRE].

[24] D.E. Kharzeev, J. Liao, S.A. Voloshin and G. Wang, *Chiral magnetic and vortical effects in high-energy nuclear collisions — A status report*, *Prog. Part. Nucl. Phys.* **88** (2016) 1 [arXiv:1511.04050] [ɪɴSPIRE].

[25] V. Koch et al., *Status of the chiral magnetic effect and collisions of isobars*, *Chin. Phys.* **C 41** (2017) 072001 [arXiv:1608.00982] [ɪɴSPIRE].

[26] K. Landsteiner, *Notes on Anomaly Induced Transport*, *Acta Phys. Polon.* **B 47** (2016) 2617 [arXiv:1610.04413] [ɪɴSPIRE].

[27] E.V. Gorbar, V.A. Miransky, I.A. Shovkovy and P.O. Sukhachov, *Anomalous transport properties of Dirac and Weyl semimetals (Review Article)*, *Low Temp. Phys.* **44** (2018) 487 [arXiv:1712.08947] [ɪɴSPIRE].

[28] X.-G. Huang and J. Liao, *Axial Current Generation from Electric Field: Chiral Electric Separation Effect*, *Phys. Rev. Lett.* **110** (2013) 232302 [arXiv:1303.7192] [ɪɴSPIRE].

[29] Y. Jiang, X.-G. Huang and J. Liao, *Chiral electric separation effect in the quark-gluon plasma*, *Phys. Rev.* **D 91** (2015) 045001 [arXiv:1409.6395] [ɪɴSPIRE].

[30] S. Pu, S.-Y. Wu and D.-L. Yang, *Holographic Chiral Electric Separation Effect*, *Phys. Rev.* **D 89** (2014) 085024 [arXiv:1401.6972] [ɪɴSPIRE].

[31] S. Pu, S.-Y. Wu and D.-L. Yang, *Chiral Hall Effect and Chiral Electric Waves*, *Phys. Rev.* **D 91** (2015) 025011 [arXiv:1407.3168] [ɪɴSPIRE].

[32] T. Sakai and S. Sugimoto, *Low energy hadron physics in holographic QCD*, *Prog. Theor. Phys.* **113** (2005) 843 [hep-th/0412141] [ɪɴSPIRE].

[33] T. Sakai and S. Sugimoto, *More on a holographic dual of QCD*, *Prog. Theor. Phys.* **114** (2005) 1083 [hep-th/0507073] [INSPIRE].

[34] E.V. Gorbar, I.A. Shovkovy, S. Vilchinskii, I. Rudenok, A. Boyarsky and O. Ruchayskiy, *Anomalous Maxwell equations for inhomogeneous chiral plasma*, *Phys. Rev.* **D 93** (2016) 105028 [arXiv:1603.03442] [INSPIRE].

[35] E.V. Gorbar, V.A. Miransky, I.A. Shovkovy and P.O. Sukhachov, *Consistent hydrodynamic theory of chiral electrons in Weyl semimetals*, *Phys. Rev.* **B 97** (2018) 121105 [arXiv:1712.01289] [INSPIRE].

[36] E.V. Gorbar, V.A. Miransky, I.A. Shovkovy and P.O. Sukhachov, *Hydrodynamic electron flow in a Weyl semimetal slab: Role of Chern-Simons terms*, *Phys. Rev.* **B 97** (2018) 205119 [arXiv:1802.07265] [INSPIRE].

[37] E.V. Gorbar, V.A. Miransky, I.A. Shovkovy and P.O. Sukhachov, *Collective excitations in Weyl semimetals in the hydrodynamic regime*, *J. Phys. Condens. Matter* **30** (2018) 275601 [arXiv:1802.10110] [INSPIRE].

[38] A.V. Sadofyev and M.V. Isachenkov, *The Chiral magnetic effect in hydrodynamical approach*, *Phys. Lett.* **B 697** (2011) 404 [arXiv:1010.1550] [INSPIRE].

[39] Y. Neiman and Y. Oz, *Relativistic Hydrodynamics with General Anomalous Charges*, *JHEP* **03** (2011) 023 [arXiv:1011.5107] [INSPIRE].

[40] T. Kalaydzhyan and I. Kirsch, *Fluid/gravity model for the chiral magnetic effect*, *Phys. Rev. Lett.* **106** (2011) 211601 [arXiv:1102.4334] [INSPIRE].

[41] G.T. Horowitz, J.E. Santos and D. Tong, *Optical Conductivity with Holographic Lattices*, *JHEP* **07** (2012) 168 [arXiv:1204.0519] [INSPIRE].

[42] M. Blake and D. Tong, *Universal Resistivity from Holographic Massive Gravity*, *Phys. Rev.* **D 88** (2013) 106004 [arXiv:1308.4970] [INSPIRE].

[43] R.A. Davison and B. Goutéraux, *Dissecting holographic conductivities*, *JHEP* **09** (2015) 090 [arXiv:1505.05092] [INSPIRE].

[44] A. Gynther, K. Landsteiner, F. Pena-Benitez and A. Rebhan, *Holographic Anomalous Conductivities and the Chiral Magnetic Effect*, *JHEP* **02** (2011) 110 [arXiv:1005.2587] [INSPIRE].

[45] Y. Bu, M. Lublinsky and A. Sharon, *Anomalous transport from holography: Part I*, *JHEP* **11** (2016) 093 [arXiv:1608.08595] [INSPIRE].

[46] Y. Bu, M. Lublinsky and A. Sharon, *Anomalous transport from holography: Part II*, *Eur. Phys. J.* **C 77** (2017) 194 [arXiv:1609.09054] [INSPIRE].

[47] S. Bhattacharyya, V.E. Hubeny, S. Minwalla and M. Rangamani, *Nonlinear Fluid Dynamics from Gravity*, *JHEP* **02** (2008) 045 [arXiv:0712.2456] [INSPIRE].

[48] S.A. Hartnoll, P.K. Kovtun, M. Muller and S. Sachdev, *Theory of the Nernst effect near quantum phase transitions in condensed matter and in dyonic black holes*, *Phys. Rev.* **B 76** (2007) 144502 [arXiv:0706.3215] [INSPIRE].

[49] S.A. Hartnoll, *Theory of universal incoherent metallic transport*, *Nature Phys.* **11** (2015) 54 [arXiv:1405.3651] [INSPIRE].

[50] R.A. Davison, B. Goutéraux and S.A. Hartnoll, *Incoherent transport in clean quantum critical metals*, *JHEP* **10** (2015) 112 [arXiv:1507.07137] [INSPIRE].

[51] B. Müller and D.-L. Yang, *Viscous Leptons in the Quark Gluon Plasma*, *Phys. Rev.* **D 91** (2015) 125010 [arXiv:1503.06967] [INSPIRE].

[52] J. Erlich, E. Katz, D.T. Son and M.A. Stephanov, *QCD and a holographic model of hadrons*, *Phys. Rev. Lett.* **95** (2005) 261602 [hep-ph/0501128] [INSPIRE].

[53] Y. Matsuo, S.-J. Sin, S. Takeuchi and T. Tsukioka, *Magnetic conductivity and Chern-Simons Term in Holographic Hydrodynamics of Charged AdS Black Hole*, *JHEP* **04** (2010) 071 [arXiv:0910.3722] [INSPIRE].

[54] K. Landsteiner and Y. Liu, *The holographic Weyl semi-metal*, *Phys. Lett.* **B 753** (2016) 453 [arXiv:1505.04772] [INSPIRE].

[55] K. Landsteiner, Y. Liu and Y.-W. Sun, *Quantum phase transition between a topological and a trivial semimetal from holography*, *Phys. Rev. Lett.* **116** (2016) 081602 [arXiv:1511.05505] [INSPIRE].

[56] K. Landsteiner, Y. Liu and Y.-W. Sun, *Odd viscosity in the quantum critical region of a holographic Weyl semimetal*, *Phys. Rev. Lett.* **117** (2016) 081604 [arXiv:1604.01346] [INSPIRE].

[57] K. Landsteiner, Y. Liu and Y.-W. Sun, *Negative magnetoresistivity in chiral fluids and holography*, *JHEP* **03** (2015) 127 [arXiv:1410.6399] [INSPIRE].

[58] Y.-W. Sun and Q. Yang, *Negative magnetoresistivity in holography*, *JHEP* **09** (2016) 122 [arXiv:1603.02624] [INSPIRE].

[59] Y. Seo, G. Song, P. Kim, S. Sachdev and S.-J. Sin, *Holography of the Dirac Fluid in Graphene with two currents*, *Phys. Rev. Lett.* **118** (2017) 036601 [arXiv:1609.03582] [INSPIRE].

[60] M. Rogatko and K.I. Wysokinski, *Holographic calculation of the magneto-transport coefficients in Dirac semimetals*, *JHEP* **01** (2018) 078 [arXiv:1712.01608] [INSPIRE].

[61] M. Rogatko and K.I. Wysokinski, *Two interacting current model of holographic Dirac fluid in graphene*, *Phys. Rev.* **D 97** (2018) 024053 [arXiv:1708.08051] [INSPIRE].

[62] M. Ammon, M. Baggioli, A. Jiménez-Alba and S. Moeckel, *A smeared quantum phase transition in disordered holography*, *JHEP* **04** (2018) 068 [arXiv:1802.08650] [INSPIRE].

[63] S.A. Hartnoll, C.P. Herzog and G.T. Horowitz, *Building a Holographic Superconductor*, *Phys. Rev. Lett.* **101** (2008) 031601 [arXiv:0803.3295] [INSPIRE].

[64] S.A. Hartnoll, C.P. Herzog and G.T. Horowitz, *Holographic Superconductors*, *JHEP* **12** (2008) 015 [arXiv:0810.1563] [INSPIRE].

[65] M. Blake, *Momentum relaxation from the fluid/gravity correspondence*, *JHEP* **09** (2015) 010 [arXiv:1505.06992] [INSPIRE].

[66] M. Blake, *Magnetotransport from the fluid/gravity correspondence*, *JHEP* **10** (2015) 078 [arXiv:1507.04870] [INSPIRE].

[67] M. Henningson and K. Skenderis, *The Holographic Weyl anomaly*, *JHEP* **07** (1998) 023 [hep-th/9806087] [INSPIRE].

[68] V. Balasubramanian and P. Kraus, *A Stress tensor for Anti-de Sitter gravity*, *Commun. Math. Phys.* **208** (1999) 413 [hep-th/9902121] [INSPIRE].

[69] M. Taylor, *More on counterterms in the gravitational action and anomalies*, hep-th/0002125 [INSPIRE].

[70] S. de Haro, S.N. Solodukhin and K. Skenderis, *Holographic reconstruction of space-time and renormalization in the AdS/CFT correspondence*, *Commun. Math. Phys.* **217** (2001) 595 [hep-th/0002230] [INSPIRE].

[71] B. Sahoo and H.-U. Yee, *Electrified plasma in AdS/CFT correspondence*, *JHEP* **11** (2010) 095 [arXiv:1004.3541] [INSPIRE].

[72] J.M. Maldacena, *The large N limit of superconformal field theories and supergravity*, *Int. J. Theor. Phys.* **38** (1999) 1113 [*Adv. Theor. Math. Phys.* **2** (1998) 231] [hep-th/9711200] [INSPIRE].

[73] S.S. Gubser, I.R. Klebanov and A.M. Polyakov, *Gauge theory correlators from noncritical string theory*, *Phys. Lett.* **B 428** (1998) 105 [hep-th/9802109] [INSPIRE].

[74] E. Witten, *Anti-de Sitter space and holography*, *Adv. Theor. Math. Phys.* **2** (1998) 253 [hep-th/9802150] [INSPIRE].

[75] S. Bhattacharyya, R. Loganayagam, I. Mandal, S. Minwalla and A. Sharma, *Conformal Nonlinear Fluid Dynamics from Gravity in Arbitrary Dimensions*, *JHEP* **12** (2008) 116 [arXiv:0809.4272] [INSPIRE].

[76] J. Hur, K.K. Kim and S.-J. Sin, *Hydrodynamics with conserved current from the gravity dual*, *JHEP* **03** (2009) 036 [arXiv:0809.4541] [INSPIRE].

[77] G. Policastro, D.T. Son and A.O. Starinets, *The Shear viscosity of strongly coupled N = 4 supersymmetric Yang-Mills plasma*, *Phys. Rev. Lett.* **87** (2001) 081601 [hep-th/0104066] [INSPIRE].

[78] P. Kovtun, D.T. Son and A.O. Starinets, *Viscosity in strongly interacting quantum field theories from black hole physics*, *Phys. Rev. Lett.* **94** (2005) 111601 [hep-th/0405231] [INSPIRE].

[79] D.T. Son and A.O. Starinets, *Viscosity, Black Holes and Quantum Field Theory*, *Ann. Rev. Nucl. Part. Sci.* **57** (2007) 95 [arXiv:0704.0240] [INSPIRE].

[80] P.K. Kovtun and A.O. Starinets, *Quasinormal modes and holography*, *Phys. Rev.* **D 72** (2005) 086009 [hep-th/0506184] [INSPIRE].

[81] S.A. Hartnoll, *Lectures on holographic methods for condensed matter physics*, *Class. Quant. Grav.* **26** (2009) 224002 [arXiv:0903.3246] [INSPIRE].

[82] C.P. Herzog, *Lectures on Holographic Superfluidity and Superconductivity*, *J. Phys.* **A 42** (2009) 343001 [arXiv:0904.1975] [INSPIRE].

[83] S.A. Hartnoll and C.P. Herzog, *Ohm's Law at strong coupling: S duality and the cyclotron resonance*, *Phys. Rev.* **D 76** (2007) 106012 [arXiv:0706.3228] [INSPIRE].

[84] G. Policastro, D.T. Son and A.O. Starinets, *From AdS/CFT correspondence to hydrodynamics. 2. Sound waves*, *JHEP* **12** (2002) 054 [hep-th/0210220] [INSPIRE].

[85] X.-H. Ge, Y. Matsuo, F.-W. Shu, S.-J. Sin and T. Tsukioka, *Density Dependence of Transport Coefficients from Holographic Hydrodynamics*, *Prog. Theor. Phys.* **120** (2008) 833 [arXiv:0806.4460] [INSPIRE].

[86] E. Megias and F. Pena-Benitez, *Holographic Gravitational Anomaly in First and Second Order Hydrodynamics*, *JHEP* **05** (2013) 115 [arXiv:1304.5529] [INSPIRE].